A THESIS SUBMITTED TO
THE GRADUATE SCHOOL OF NATURAL AND APPLIED SCIENCES
OF ÇANKIRI KARATEKİN UNIVERSITY

INVESTIGATION OF THE ULTRAVIOLET-VISIBLE (UV-VIS) SPECTRUM AND MOLECULAR STRUCTURE OF LOPINAVIR COMPOUND USED IN THE TREATMENT OF COVID-19 BY COMPUTATIONAL CHEMISTRY METHODS

IN PARTIAL FULFILLMENT OF THE REQUIREMENTS
FOR
THE DEGREE OF MASTER OF SCIENCE
IN
PHYSICS

BY

ALI JAWAD KADHIM AL-JANABI

ÇANKIRI

2023

INVESTIGATION OF THE ULTRAVIOLET-VISIBLE (UV-VIS) SPECTRUM AND MOLECULAR STRUCTURE OF LOPINAVIR COMPOUND USED IN THE TREATMENT OF COVID-19 BY COMPUTATIONAL CHEMISTRY METHODS

By Ali Jawad Kadhim AL-JANABI

June 2023

We certify that we have read this thesis and that in our opinion it is fully adequate, in scope and in quality, as a thesis for the degree of Master of Science

Advisor **:** Prof. Dr. Çiğdem YÜKSEKTEPE ATAOL

Examining Committee Members:

Chairman **:** Prof. Dr. Çiğdem YÜKSEKTEPE ATAOL
Physics
Çankırı Karatekin University

Member **:** Prof. Dr. Sebahaddin ALPTEKİN
Physics
Çankırı Karatekin University

Member **:** Prof. Dr. Sibel DEMİR KANMAZALP
Technical Sciences, Biomedical Device Technology
Gaziantep University

Approved for the Graduate School of Natural and Applied Sciences

Prof. Dr. Hamit ALYAR
Director of Graduate School

I hereby declare that all information in this document has been obtained and presented in accordance with academic rules and ethical conduct. I also declare that, as required by these rules and conduct, I have fully cited and referenced all material and results that are not original to this work.

Ali Jawad Kadhim AL-JANABI

ABSTRACT

INVESTIGATION OF THE ULTRAVIOLET-VISIBLE (UV-VIS) SPECTRUM AND MOLECULAR STRUCTURE OF LOPINAVIR COMPOUND USED IN THE TREATMENT OF COVID-19 BY COMPUTATIONAL CHEMISTRY METHODS

Ali Jawad Kadhim AL-JANABI

Master of Science in Physics

Advisor: Prof. Dr. Çiğdem YÜKSEKTEPE ATAOL

June 2023

The compound Lopinavir, which is used as an antiviral agent in COVID-19 and AIDS diseases caused by the coronavirus and HIV-1 viruses, is among the main drugs used to treat patients with such diseases. The molecular structure of the Lopinavir compound with the chemical formula $C_{37}H_{48}N_4O_5$ was investigated using computational chemistry methods. Density Functional Theory, which gives very good results for organic compounds, was used in the calculations. The molecular structure of the Lopinavir compound was obtained in the ground state from both gas and solvents with different dielectric constants and dipole moments, such as ethanol, acetone, chloroform, and water. The molecular structure of the Lopinavir compound was first optimized in gas and different solvent environments using the B3LYP/6-311G(d, p) and B3LYP/6-311+G(d, p) methods. A molecular electrostatic potential map was obtained using the optimized molecular structures of the Lopinavir compound. Molecular orbital energy values of the molecular structure of the Lopinavir compound were obtained, percentage contributions of functional groups to molecular orbital energy levels were calculated and global reactivity parameters were found. Ultraviolet-Visible spectra of the Lopinavir molecular structure in the excited state for both gas and different solvent environments have been obtained using Time-Dependent Density Functional Theory.

2023, 57 pages

Keywords: Covid-19, Density functional theory, Lopinavir, UV-vis spectra

ÖZET

COVİD-19 TEDAVİSİNDE KULLANILAN LOPİNAVİR BİLEŞİĞİNİN MOLEKÜLER YAPISININ VE ULTRAVİYOLE-GÖRÜNÜR BÖLGE (UV-VİS) SPEKTRUMUNUN HESAPLAMALI KİMYA YÖNTEMLERİ İLE İNCELENMESİ

Ali Jawad Kadhim AL-JANABI

Fizik, Yüksek Lisans

Tez Danışmanı: Prof. Dr. Çiğdem YÜKSEKTEPE ATAOL

Haziran 2023

Korona ve HIV-1 virüslerinin sebep olduğu COVID-19 ve AIDS hastalıklarında antivirüs olarak kullanılan Lopinavir bileşiği bu tür hastalıklarda hastaları tedavi etmek için kullanılan başlıca ilaçlar arasındadır. $C_{37}H_{48}N_4O_5$ kimyasal formüle sahip Lopinavir bileşiğinin moleküler yapısı hesaplamalı kimya yöntemleri kullanılarak araştırılmıştır. Hesaplamalarda organik bileşikler için oldukça iyi sonuçlar veren Yoğunluk Fonksiyonel Teorisi kullanılmıştır. Lopinavir bileşiğinin moleküler yapısı taban durumda hem gaz hem de etanol, aseton, kloroform ve su gibi farklı dielektrik sabiti ve dipol momente sahip çözücü ortamlarından elde edilmiştir. Lopinavir bileşiğinin moleküler yapısı ilk olarak gaz ve farklı çözücü ortamlarında B3LYP/6-311G(d, p) ve B3LYP/6-311+G(d, p) metotları seçilerek optimize edilmiştir. Lopinavir bileşiğinin optimize edilen moleküler yapıları kullanılarak moleküler elektrostatik potansiyel haritası elde edilmiştir. Lopinavir bileşiğinin moleküler yapısının moleküler orbital enerji değerleri elde edilmiş, moleküler orbital enerji seviyelerine fonksiyonel grupların yüzde katkıları hesaplatılmış ve küresel reaktivite parametreleri bulunmuştur. Lopinavir moleküler yapısının hem gaz hem de farklı çözücü ortamları için uyarılmış durumda Zamana Bağlı Yoğunluk Fonksiyonel Teorisi kullanılarak Ultraviole-Görünür Bölge spektrumları elde edilmiştir.

2023, 57 sayfa

Anahtar Kelimeler: Covid-19, Yoğunluk fonksiyonel teorisi, Lopinavir, UV-vis spektra

PREFACE AND ACKNOWLEDGEMENTS

I would like to thank my thesis advisor, Prof. Dr. Çiğdem YÜKSEKTEPE ATAOL, for her patience, guidance, and understanding.

Ali Jawad Kadhim AL-JANABI

Çankırı-2023

CONTENTS

LIST OF SYMBOLS

A	Absorption
a.u.	Atomic unit
η	Chemical hardness
μ_{CP}	Chemical potential
°C	Degree celsius
χ	Electranegativity
$\rho(r)$	Electron density
eV	Electronvolt
ω	Electrophilicity index
ΔE	Energy gap
$E_{xc}[\rho]$	Exchange–correlation energy
$V_{xc}(r)$	Exchange–correlation potential
ν	Frequency
S	Global softness
$T[\rho]$	Kinetic energy
mJ	Millijoule
mL	Milliliter
ng	Nanogram
%	Percentage
h	Plank's constant
V_{ext}	The external potential
T	Transmission
ψ	Wave function
Λ	Wavelength

LIST OF ABBREVIATIONS

CIF	Crystallographic information file
COVID-19	Coronavirus disease 2019
CoVs	Coronaviruses
DFT	Density functional theory
DOS	Density of state
EA	Electron affinity
FMOs	Frontier molecular orbitals
GTO	Gaussian-type orbitals
HF	Hartree-Fock
HOMO	Highest occupied molecular orbital
HPLC	High-performance liquid chromatography
IDSA	Infectious diseases society of America
IP	Ionization potential
KS	Khon-Sham
LOPV	Lopinavir
LUMO	Lowest unoccupied molecular orbital
MEP	Molecular electrostatic potential
NMR	Nuclear magnetic resonance
STO	Slater-type orbitals
TD	Time-dependent
UV	Ultraviolet
WHO	World health organization

LIST OF FIGURES

LIST OF TABLES

1. INTRODUCTION

Several cases of severe pneumonia, none of which could be explained, were reported in Wuhan, China, in December 2019. Many groups, including governments and academics, looked into it. The World Health Organization (WHO) officially designated the illness brought on by the 2019 novel coronavirus (2019nCoV) on February 11, 2020 (Yang *et al.* 2020) as coronavirus disease 2019 (COVID-19). Worldwide, there have been around 151.000.000 cases and 621.000 fatalities as of July 23, 2020. Humans are a host for a class of viruses called coronaviruses (Zhao *et al.* 2019). SARS-CoV and MERS-CoV have caused pandemics. CoVs are glycoprotein-containing, enveloped, positive-sense RNA viruses. Human disorders caused by CoVs include respiratory, digestive, neurological, and brain diseases (Containing 2020, Lippi *et al.* 2020). A genomic investigation of a Wuhan COVID-19 patient found 89% nucleotide identity with bat SARS-like-CoVZXC 21% and 82% with human SARS-CoV. The 2019nCoV virus has a single-stranded RNA genome with 29.891 nucleotides encoding 9.860 amino acids. 2019nCoV invades lung cells via the renin-angiotensin system, according to studies (ACE2) (Nelson 2020).

Hu *et al.* (2022) describe coronaviruses (CoVs) as follows: "CoVs are single-stranded positive-sense RNA enveloped viruses with a 5′-cap and 3′-poly-A tail." CoVs infect vertebrates including humans and birds and typically manifest as respiratory and gastrointestinal symptoms in those hosts. SARS-CoV, MERS-CoV, and SARS-CoV-2, which cause severe acute respiratory syndrome, are three of seven human coronaviruses (Artika *et al.* 2020, Gorbalenya *et al.* 2006). The International Committee on Taxonomy of Viruses' latest report classifies SARS-CoV-2 and SARS-CoV as Sarbecoviruses. SARS coronavirus type 2 (SARSCoV-2) causes COVID-19, which has killed millions and devastated society. Researchers have put a lot of time and energy into developing vaccines, repurposing existing drugs, and finding new treatments for this epidemic (Mirza and Froeyen 2020). COVID-19 primary prevention vaccines target the viral spike (S) protein. New SARS-CoV-2 variations (e.g., Delta and Omicron) have caused high-

frequency nucleic acid and amino acid changes in the S protein, which threatens vaccination efficacy and mutation-mediated resistance (Raj *et al.* 2013).

Lopinavir (LOPV) is an antiviral medicine that is used to treat coronavirus. The molecule has the chemical formula 2S-N-[(2S,4S,5S)]One that is derived from acetamido-5-[2-(2,6-dimethylphenoxy)]-4-hydroxy-1,6-diphenylhexan-2-yl]-3-methyl-2-(2-oxo-1,3diazinan-1-yl)butanamide. The structure of this substance is represented by the chemical formula $C_{37}H_{48}N_4O_5$, and its molecular weight as a whole is 628.80. Figure 1.1 depicts the Lopinavir structure (Gorbalenya *et al.* 2020). Human immunodeficiency virus proteinase is inhibited, so the gag-pol polyprotein is not cleaved, and the virus remains in an inactive, non-infectious form. It dissolves easily in acetonitrile, methanol, and chloroform, but it doesn't even come close to dissolving in water. Lopinavir is official in USP 2010 and IP 2007 the official method of assay in both IP 2007 and USP 2010 is high-performance liquid chromatography (HPLC) (Thakkar and Patel 2010). Chromatographic techniques, including HPLC with a variety of detectors and mobile phase compositions, are included among the documented methods of analysis (Donato *et al.* 2006, Donato 2008). Chromatographic methods are tedious and time-consuming. Thus far, only one UV spectrophotometry-based method is reported for the estimation of the Lopinavir (Guideline 2005). However, the reported ultraviolet (UV) method is found to have less sensitivity as evidenced by the high value of the limit of quantitation (LOQ) (10 µg/mL).

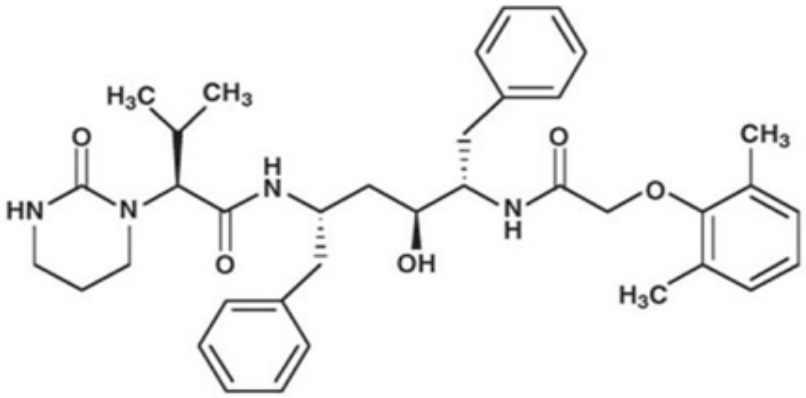

Figure 1.1 The chemical structure of the Lopinavir

This thesis uses Density Functional Theory (DFT) to clarify the molecular structure of the Lopinavir molecule, the structure of which has not been clarified to a great extent in the literature. Its molecular structure has been fine-tuned to function optimally in gas and various solvents. The calculations employed both the B3LYP/6-311G(d, p) and B3LYP/6-311+G(d, p) approaches. Ultraviolet-Visible (UV-Vis) spectroscopy methods were used to obtain a map of the molecular electrostatic potential (MEP), values for molecular orbital energies, global reactivity parameters, and absorption wavelengths for gas and solvent environments using the optimized structures.

2. LITERATURE REVIEW

In this thesis, it is focused on the lopinavir molecule. Using gradient RP-HPLC, Chitturi *et al.* (2008) analyzed several related chemicals (RS4-RS10) found in lopinavir pharmacological material at concentrations between 0.03% and 0.1%. LC-MS analysis uncovered the linked compounds. Mass, ^{1}H-NMR, and FT-IR spectrum data were used to identify and isolate these similar compounds. The separation was carried out in gradient elution mode using 0.02 M KH_2PO_4 (pH 2.5): acetonitrile as the mobile phase on a YMC Pack ODS-AQ (250 mm, 4.6 mm, 5m) column maintained at 45 C. For detection, we employed a PDA detector with a 210 nm setting. The detection and quantitation limits for the method ranged from 0.028 ng/mL to 0.063 ng/mL and from 0.084 ng/mL to 0.192 ng/mL, respectively, as demonstrated by the analyzed validation elements. Regular analysis for quality control and stability testing of lopinavir drug material can be performed using this method.

Czech *et al.* (2022) Antiviral drug concentrations have increased in waste water and hospital effluents as a result of the usage of lopinavir and ritonavir alone or in combination with other medications. It is anticipated that the removal efficiency of several antiviral medications is low (20%) in typical wastewater treatment plants. Both lopinavir and ritonavir are extremely harmful to aquatic creatures over the long term, as evidenced by their high predicted no-effect concentrations (PNECs; inngL1). This means that lopinavir and ritonavir should be carefully monitored and efficiently eliminated from all water and waste-water samples since they are now considered to be among the most important antiviral medications.

Heidari (2020) Among antiretrovirals, ritonavir stands out as a protease inhibitor. Lopinavir/ritonavir is a fixed-dose combination used to treat HIV infections; both drugs are protease inhibitors. In this study, researchers looked into a liquid sample of Ritonavir using stimulated FT-Raman Bio spectroscopy. Focusing a beam of Nd: YAG's second harmonic laser onto the sample causes it to emit diffractions that are picked up by an Echelle spectrometer and an ICCD detector, which records them as stimulated FT-Raman waves. Stimulated FT-Raman signals decreased with increasing energy above the liquid

sample's breakdown threshold; at 20 mJ and above, the signals completely vanished. The stimulated FT-Raman signal increased from 2.6 (mJ) to 16 (mJ) as the laser beam energy was increased.

Azadparvar *et al.* (2022) Tetrahydroaltersolanol ($C_{16}H_{20}O_7$) and its fluorinated derivatives have their structural, optoelectronic, and biological properties predicted by (DFT) and molecular docking methods. It is demonstrated that the direct energy gap of the pure $C_{16}H_{20}O_7$ molecule is approximately 3.1 eV. The electronic energy gap narrows when the F atom is substituted into the A category, but remains unchanged in the B category. In the A class, different F atom substitutions shifted the molecule's behavior from insulator to semiconductor. The electrical characteristics of the pure molecule were found to be F-site dependent. As the energy gap between two atoms or molecules decreases, the molecules become better able to conduct electricity and exchange charges with one another. Chemical reactivity is enhanced by the F atom substitution compared to the pure $C_{16}H_{20}O_7$ molecule with a high energy gap, which has poor reactivity. The obtained data highlights the importance of the F-O bonds in the trifurcation bonds of $C_{16}H_{19}O_7$ (F14), $C_{16}H_{19}O_7$ (F16), and $C_{16}H_{19}O_7$ (F17) molecules in combating COVID-19, HIV, and HTLV proteases, in that order. The utilization of optical spectra, including dielectric functions, electron energy-loss spectroscopy, index of refractive, coefficient of extinction, and reflection spectra, has demonstrated that the fluorinated derivatives of $C_{16}H_{20}O_7$ within the B category exhibit potential for application in the advancement of innovative pharmaceuticals.

3. MATERIALS AND METHODS

Lopinavir (LOPV) is a chemical with the formula ((2S)-N-[(2S,4S,5S)])-5-[[2-(2,6-dimethylphenoxy)acetyl]amino]-4-hydroxy-1,6-diphenylhexan-2-yl]. Researchers have elucidated the structure of 3-methyl-2-(2-oxo-1,3-diazinan-1-yl)butanamide), a protease inhibitor utilized in HIV-1 and COVID-19 therapies. The present study employed the computational chemistry technique of DFT to calculate various properties of the molecular structure, molecular electrostatic potential map, molecular orbital energy values, and reactivity parameters of the LOPV compound. Theoretical UV-vis spectra of the LOPV were obtained using Time-Dependent (TD)-DFT calculations. The Gaussian 09 software was utilized to execute the calculations (Frisch *et al.* 2009). All the computations were carried out using the molecular visualization program Gaussview. The LOPV compound was subjected to ground-state optimization in various environments, including gas, ethanol, acetone, chloroform, and water. The optimization was conducted using the polarised basis set 6-311G(d, p) and the diffuse polarised basis set 6-311+G(d, p). Becke's three-parameter functional, commonly abbreviated as B3, is a mathematical model used in computational chemistry to describe the exchange-correlation energy of a system (Becke 1993) is an example of such a functional; the exchange functional is formed by linearly combining the Hartree-Fock, local, and gradient-corrected exchange terms. Combining Lee's (Lee *et al.* 1988) correlation functionals with the B3 hybrid functional. The computations made use of the B3LYP base function, one of the hybrid functionals that provide excellent results for organic molecules.

Gaussian, created by Gaussian, Inc., is a commercially accessible suite of quantum chemistry software. The software is compatible with a wide variety of platforms, including Microsoft Windows. Web-based interface tools, such as Web MO, provide another avenue of access. The North Carolina School of Computational Chemistry provides its faculty, staff, and student researchers with access to Gaussian, the most cutting-edge program in the field. G09 (Gaussian 09) has been released. The number "09" relates to the year in which the program was first released, which was in 2009. Version G09 is not the most recent (Frisch *et al.* 2009).

Gauss vision is an operating system used to load input files for Gaussian software and to display Gaussian program output files in a dimensional picture. It is not a calculating program, but it simplifies work with Gaussian programs and provides three significant advantages to users.

First: It lets the user draw molecules of any size, as well as rotate, transfer, and change their size with the mouse.

Second: The Gaussian view enables and performs a large number of Gaussian calculations, preparing the complicated input for regular work and sophisticated methods.

Third: The Gaussian view enables the examination of Gaussian computation results through the use of a variety of geometrical techniques, including the following: (Balanced molecular patterns, molecular orbitals, and electronic density surfaces) (Parr and Yang 1995).

3.1 Computational Chemistry

Computational chemistry expresses chemistry in mathematical ways. It is a method that investigates molecular structures. In this thesis, DFT and Hartree-Fock (HF) methods, which are highly preferred in computational chemistry, were used.

The Thomas-Fermi model (Thomas 1927, Fermi 1927) was used to establish Functional Density Concept (DFT), which was afterward established by the Hohenberg-Kohn theory (Hohenberg and Kohn 1964). The Kohn-Sham theorist, in particular, has laid the groundwork for the use of DFT in mathematical modeling. It was not until the early 1980s that real progress in applying Kohn-Sham's theory to chemistry was made. Although there is substantial older literature on atomic processes, early molecular applications were hampered by mathematical indecisions. The DFT was used first in chemistry in the1960s using numerical methods adjusted from the solid state vocabulary called scattered-wave. These were found to be inadequate for discussing finite molecules. Potential energy

curves and precise densities can not be estimated for one-electron spectrometric characteristics. To control the nonanalytical exchange-correlation troubles, numerous corresponding characteristic methods were merged with mathematical optimization methods throughout the 1970s, and by 1980, credible computational techniques for DFT chemical reactions were eventually in position (Kohn and Sham 1965).

3.1.1 Density functional theory (DFT)

When it comes to computing the electronic structure of matter, (DFT) is one of the most well-liked and fruitful quantum mechanical techniques (Valone 2010). The Thomas-Fermi model, established by Thomas and Fermi in 1927, was utilized as a functional precursor to the density principle. Thomas and Fermi used a plot of kinetic energy vs electron density to estimate the atomic energy. According to Rogers (2003) and also Fitts (1999), (DFT) has the capability to make prognostications regarding various molecular characteristics such as vibrational frequencies, ionization energies, electric and atomization energies, reaction pathways, and magnetic properties. DFT approaches are growing in popularity due to the significant reduction in CPU time required to provide results that are competitive with those produced by ab initio methods. In the computation of energy, the DFT methodology employs the electron density as opposed to the wave function utilised in other HF-derived methodologies (Sholl and Steckel 2011, Bransden and Joachain 2003). The (DFT) is utilized to ascertain the characteristics of a vast assemblage of particles in relation to their electron density, ρ(r). A state's electron density is the total number of electrons in a given volume of that state. Irrespective of the electron count within the system, it necessitates solely three coordinates, as evidenced below in Equation (3.1) (Mueller 2007).

$$N = \int \rho(\vec{r})\, d\vec{r} \tag{3.1}$$

When the electron is far enough from the nucleus that its probability of being there approaches 0, the density of electrons in that region is said to be infinite. As the number of electrons rises, theoretically speaking, the wavefunction approaches get substantially more difficult (Kohanoff and Gidopoulos 2003).

The basis of DFT lies in the ground state energy, whereby the electron density determines all other electronic properties in the ground state. Moreover, when the total energy is limited, the exact ground state of the system corresponds to the electronic density (Mueller 2007).

All calculations in the thesis study were made with the DFT method.

3.1.2 Hartree Fock (HF) theory

The Schrödinger equation is commonly utilized to solve for the behaviour of electrons in a given system. However, due to the complexity of the equation, approximations are often employed. One such widely recognised approximation is the Hartree-Fock method. The fundamental principle of molecular orbital (MO) theory posits that every electron within a molecule possesses an individualised single-particle function, or orbital, that remains unaffected by the concurrent movements of the other electrons (Young 2004). Hartree assumed that the total wave function could be generally approximated as a series of one electron wave functions (Rogers 2003). The so-called Hartree–Fock equations as in Equation (3.2):

$$\hat{f}_i \Psi_i = \varepsilon_i \Psi_i \qquad (3.2)$$

Where Ψ_i is an eigenfunction of the operator $\hat{f}_i$, which is also known as the Fock operator and ε_i is the corresponding energy.

The calculated approximations of energy are all larger than or equivalent to the true energy. Hartrees are the units used to determine the energies (1 Hartree=27.2116 eV) (Fock 1930).

The Hartree-Fock approximation states that the Slater determinant can express the wave function of an n-electron system. These determinant states that all electron spins follow

the Pauli Exclusion Principle. Hartree-Fock wave functions are often Slater determinants as in Equation (3.3).

$$\Psi\,(1.2.\ldots.n) = \frac{1}{\sqrt{n!}}\begin{vmatrix} \Psi_1(\chi_1) & \Psi_2(\chi_1) & \ldots & \Psi_n(\chi_1) \\ \Psi_1(\chi_2) & \Psi_2(\chi_2) & \ldots & \Psi_n(\chi_2) \\ \vdots & \vdots & \ddots & \vdots \\ \Psi_1(\chi_n) & \Psi_1(\chi_n) & \ldots & \Psi_n(\chi_n) \end{vmatrix} \quad (3.3)$$

where Ψ is the electronic wave function, and $\frac{1}{\sqrt{n!}}$ is a normalization factor (Young 2004).

3.1.3 Hohenberg-Kohn theory

The Hohenberg-Kohn work simplified the issue of solving the many-body Schrödinger equation to a density functional minimization goal. They established in 1964 that the ground-state electron density could accurately assess numerous ground-state electron systems (ρ_r) (Rogers 2003, Valone 2010, Cramer 2013).

Theorem I: The ground state energy of a system with multiple electrons is a distinct and universal function of the electron density in the ground state (ρ_r).

Theorem II: In a system with multiple electrons, the electron density in its ground state (represented as ρr) is optimised to minimise the function of the system's the ground state energy.

Theorems dictate that ground state characteristics of a system with multiple electrons can be explicated through the ground state electron density (ρ(r)). The functional E_V that characterises the ground state's energy can be delineated in the Equation (3.4) manner:

$$E_V[\rho] = \int \rho(\vec{r})\, V_{ext}(\vec{r}) d\vec{r} + F_{HK}[\rho] \quad (3.4)$$

The external potential, denoted by V_{ext}, and the functional F_{HK}, which encompasses the kinetic energy and electron-electron interactions, are both dependent on the electron density ρ(r) and require a determination as in Equation (3.5) (Koch and Holthausen 2015, Parr and Yang 1995):

$$F_{HK}[\rho] = T[\rho] + E_{NC}[\rho] + J[\rho] \quad (3.5)$$

Where $T[\rho]$ is the kinetic energy, $E_{NC}[\rho]$ is the non-classical electron–electron interaction energy, and $J[\rho]$ is the classical Coulomb energy.

The HK theorem postulates the existence of F_{HK}, albeit without a precise understanding of its actual form, necessitating the use of approximations (Lipkowitz and Boyd 2009).

3.1.4 Kohn-Sham equations

A noninteracting system can be found in the real system with the ground state density ρ(r). This noninteracting system possesses the same ρ(r). The Equation (3.6) denoted as can be reformulated as follows (Hutter 2005):

$$F[\rho] = T_S[\rho] + J[\rho] + E_{NC}[\rho] \quad (3.6)$$

The expression "where $T_S[\rho]$ is the kinetic energy of a noninteracting electron system" denotes the kinetic energy of a system of electrons that do not interact with each other. A solitary Slater determinant of orbitals characterises the electron density of a non-interacting system.

The DFT exchange–correlation energy $E_{xc}[\rho]$ of interacting electron system can be defined in the form of Equation (3.7) and Equation (3.8).

$$E_{xc}[\rho] = T[\rho] - T_S[\rho] + E_{NC}[\rho] \quad (3.7)$$

$$V_{xc}(r) = \frac{\delta E_{xc}[\rho]}{\delta \rho_{(r)}} \quad (3.8)$$

Where $V_{xc}(r)$ is the exchange–correlation potential.

Equations (3.8) The Kohn-Sham equations, also referred to as the KS equations, are characterised by formal exactitude and a solitary unknown term, $E_{xc}[\rho]$. The Kohn-Sham approach is a widely recognised methodology that has been adopted for various applications (Lipkowitz and Boyd 2009, Jones 2006).

The physics of the Kohn-Sham equation is unlike that of the Schrödinger equation. The significance of Kohn-Sham equations consists that, they reduced an interacting many-body problem to a set of independent equations which describes the state of a single electron in the effective potential of other electrons.

The principal obstacle encountered in density functional theory (DFT) pertains to the exchange-correlation energy (E_{xc}), which is a mathematical construct. The term "exchange and correlation interactions" refers to the combined effects of the Pauli exclusion principle, which governs the behaviour of electrons with opposite spin orientations, and the instantaneous reaction between electrons with the same spin orientation. The exact solution of the system is attainable provided that the exchange-correlation function is precisely determined. As previously mentioned, the differentiation of the Hamiltonians of non-interacting single-electron systems from those of interacting many-electron systems results in the derivation of this particular function (Mueller 2007).

3.2 Basis Sets

The shape of orbitals surrounding an atom is determined by a set of functions referred to as a "basis set." Linear combinations of basis functions and angular functions are utilised to construct molecular orbitals and complete wave functions. A fixed basis is utilised by most semiempirical methods. The utilization of a basis set is a prerequisite for density functional theory and ab initio calculations. Although it is possible to generate a basis set

from the beginning, the majority of computations employ pre-established basis sets. The selection of the calculation method and basis set are critical factors in determining the accuracy and validity of the outcomes obtained (Springborg 2000).

3.2.1 Slater-type orbitals (STOs)

For simple tasks, it seems like a no-brainer. The functions are exponential approximations of the hydrogen atom's eigenfunctions. One major drawback of (STO) is the difficulty in computing many-center integrals such as coulomb and HF- exchange terms (STO). As a result, it has no place in modern wave function-based quantum chemistry codes (Lipkowitz and Boyd 2009).

3.2.2 Gaussian-type orbitals (GTOs)

The many-center integrals can be efficiently calculated analytically using the (GTO) function, making it a staple in HF and related methods. To enhance GTO basis sets (CGF), it is usual to practise to utilize a contracted GTO basis set, in which a large number of primitive Gaussian functions are combined to produce a contracted Gaussian function. In contrast to the STO function, the GTO gives less weight to the tail of the nuclear wave. To attain the same precision with GTOs, almost three times as many STOs are required. One of the benefits of the Gaussian basis set is that the sum of any two Gaussian functions is a third Gaussian function. Thus, the Gaussian functions' analytic solution can be used for the calculation of Coulomb and HF-exchange terms. There are many different types of Gaussian basis sets, including minimum basis sets, split valence sets, Polarisation and Diffuse Functions, and others (Young 2004, Rogers 2003).

3.2.2.1 Minimal basis sets

The minimal basis set refers to the smallest possible set of basis functions X that can effectively represent the ground state electrons of each atom in a given molecule. The notation STO-NG is commonly used to refer to minimal basis sets, wherein the value of

n signifies the count of Gaussian primitive functions utilised for the formation of a single basis function. The range of n is typically between 2 and 6. The basis sets in question exhibit an equivalence between the number of Gaussian primitives comprising the core and valence orbital angular momentum. Although minimal basis sets are less expensive than their larger counterparts, they typically produce imprecise results that are not appropriate for scholarly publication (Minkin 1999, Kampen *et al.* 1999).

3.2.2.2 Split-valence basis sets

Minimal basis sets, expressed as STO-NG basis sets, see all electrons as equal, whereas these electrons have different roles in atomic or molecular systems. The notation for the carbon atom is $1s^2\ 2s^2\ 2p^2$. These electrons can be divided into inner shell (nucleus) and outer shell (valence) electrons. If we look at the 1s and 2s orbitals of carbon, it is seen that they differ from each other in size. A solution has to be developed to describe that the inner shell electrons are not equal to the outer shell electrons. This solution is to calculate the core electrons more roughly and the valence electrons more carefully. This can be done by developing STOs with minimal basis sets.

These base sets are Double Zeta (DZ) base sets with two zeta values. There are also triple and quadruple (Triple and quadruple (TZ, QZ)) basis sets. Generally, these base sets are referred to as Split Valence base sets. Here, as in minimal basis sets, Gaussian function approximation is used for Slater Type Orbitals. Examples of these base sets are 3-21G, 6-31G, 6-311G. If the 3-21G base set is to be examined, the first number here, 3, calculates the core electrons using the STO-3G base set, the 21 in the second part says that the STO-2G and STO-1G base sets will be used with double zeta approximation for the valence electrons (Yüksektepe 2009).

3.2.2.3 Polarization and diffuse basis sets

To improve the findings, polarization functions must be added to the basis set (Dorsett and White 2000, Gotwals and Sendlinger 2007). Higher angular momentum functions for

heavier atoms, such as d- and f-type functions, and p- and d-type functions for hydrogen and helium atoms are known as polarization functions (Reimers 2011, Santos *et al.* 2005, Kwon *et al.* 2004). By enabling the orbital form to shift, the base set becomes more versatile (i.e., becomes polarized in one direction). In systems containing hydrogen, such as hydrogen bonding and proton transfers, polarization functions, which allow the s orbital to diverge from its regular spherical form, are beneficial. Polarization functions are commonly used because they produce more precise calculated geometric shapes and vibrational frequencies (Reimers 2011, Sherrill 2002). Polarization functions are added in brackets after the contraction scheme, whereas diffuse functions are denoted by '+'. As an example, it can be given 6-311G(d, p) and 6-311+G(d, p) for the polarized split valance basis set and for the diffuse polarized split valance basis set, respectively.

3.3 Spectroscopy

A molecular structure can be characterized using spectroscopic methods. The main of these methods are Raman, NMR FT-IR, and UV-vis spectroscopic methods. In this thesis, theoretical UV-vis spectroscopy was studied using Gaussian programming.

3.3.1 Raman spectroscopy

Raman spectroscopy, a type of spectroscopy, is founded on the principle of inelastic scattering of monochromatic light, typically emanating from a laser source. The sample takes in laser photons and then emits them again. The production of Raman shifting photons is contingent upon the vibration state of the molecule, with higher or lower energy levels being observed accordingly. While anti-Stokes radiation possesses a higher amount of energy compared to Rayleigh radiation, the opposite is not applicable. Consequently, the Raman shift pertaining to the Stokes and anti-Stokes characteristics serves as a precise indicator of the data regarding the energies of vibrations and rotations that are present in the scattered radiation acquired through the Raman effect. This, in turn, is reliant on the constituent atoms or ions that make up the molecule, the chemical bonds that exist between them, and other related factors (Cutnell *et al.* 2021).

3.3.2 Nuclear magnetic resonance (NMR) spectroscopy

Nuclear magnetic resonance (NMR) spectroscopy is a scientific technique that leverages the magnetic characteristics of individual atomic nuclei. The chemical and physical properties of an atom or molecule are determined by its composition. Nuclear magnetic resonance has been widely adopted as the preferred method due to its ability to yield a vast array of information regarding a molecule's structure, dynamics, reaction state, and chemical environment. The resonance frequency of an atom in a molecule is influenced by the intermolecular magnetic field, which provides insights into the electronic structure of the molecule. Chemists and biochemists utilise NMR spectroscopy to investigate the properties of organic molecules, although it has the potential to be employed in the analysis of any substance containing nuclei with spin. The analysis of various entities, ranging from minute molecules scrutinised through proton or carbon-13 NMR spectroscopy in a solitary dimension to extensive proteins or nucleic acids investigated in three or four dimensions, is deemed acceptable. Nuclear magnetic resonance (NMR) spectroscopy has a significant impact on the scientific community due to its broad applicability to various specimens, encompassing both liquid and solid states. The absorption of electromagnetic radiation at a frequency specific to the isotope occurs in NMR active nuclei (such as ^{1}H or ^{13}C) due to the presence of magnetic fields (Pavia *et al.* 2014).

3.3.3 Infrared spectroscopy

Normal oscillations that are accompanied by changes in dipole moments are active and may be seen in the range of infrared radiation. The vibration of a molecule is modeled by normal modes of simple harmonic oscillators to absorb and emit the energy. The Infrared IR spectrum is electromagnetic radiation in the range of $(1-5)\times 10^{3}\ \mathrm{cm}^{-1}$ (Sadasivam and Kumaresan 2011).

There are three degrees of freedom in translational motion for the N-atom system during absorption and three degrees of freedom in vibration for (3N-6) ring molecules. Grant (2002) distinguishes between fundamental and nonfundamental oscillatory bands when

describing a system's oscillations. The fundamental bands are supplemented by additional dipole moment variants, which can be classified as stretch, deformation, wagging, twisting, rocking, and bending vibrations, respectively, depending on their magnitude. In contrast, the strength of overtones, hot bands, and fundamental bands is quite modest (Ketterer *et al.* 2011). For the vibration analysis to hold, the first derivative of the energy to the atomic displacement must be zero. Higher-order saddle point analysis and transition state analysis are also correct.

3.3.3.1 Ultraviolet-visible (UV-Vis) spectroscopy

Spectrophotometry is the study of an electromagnetic wave's interaction with matter. It started with an examination of the wavelength diffusion of the visible region by a prism. The concept was broadened to provide relationships that included differences in radiant energy with spectral distribution. The emission spectrum of a wavelength or frequency-dependent response is used to represent spectroscopic data. Spectroscopy is categorized into two kinds.

- Methods based on photon-to-sample energy transfer
- Reflection, diffraction, and scattering from specimens that change the amplitude, phase difference, polarizability, or direction of propagation of electromagnetic waves.

Spectroscopy has developed as a promising technique for experiment results and analyses in research labs and industries over the decades. Analysts primarily respect this method as an obvious solution. The goal should be to use these spectrophotometric methods in control and industrial labs, as well as to develop fully reproducible methods. Spectrophotometry is an essential physical device that makes utilization of light in the ultraviolet, visible, and infrared light spectrums of electromagnetic waves. A linear relationship exists between absorbance, absorber concentration in solution, and path length according to the Beer-Lambert law (Gandhimathi *et al.* 2012).

When light is radiant on a specimen, it absorbs the energy from the incident beam. As a function of wavelength, the absorbance or transmittance spectrum of the light absorbed or transmitted by the sample is formed.

The Lambert-Beer rule, depicted in Figure 3.1, is a fundamental concept of statistical analysis that creates that a solution's absorption spectrum scales straight with a concentration of the analyte. The absorption (A) for a given wavelength is characterized as the absorbance values of the absorbing substance (M^{-1} cm^{-1}), b is the distance of the sample holder and c is the content of the solvent (M) as in Equation (3.9) (Pavia *et al*. 2014).

$$A = a.b.c \tag{3.9}$$

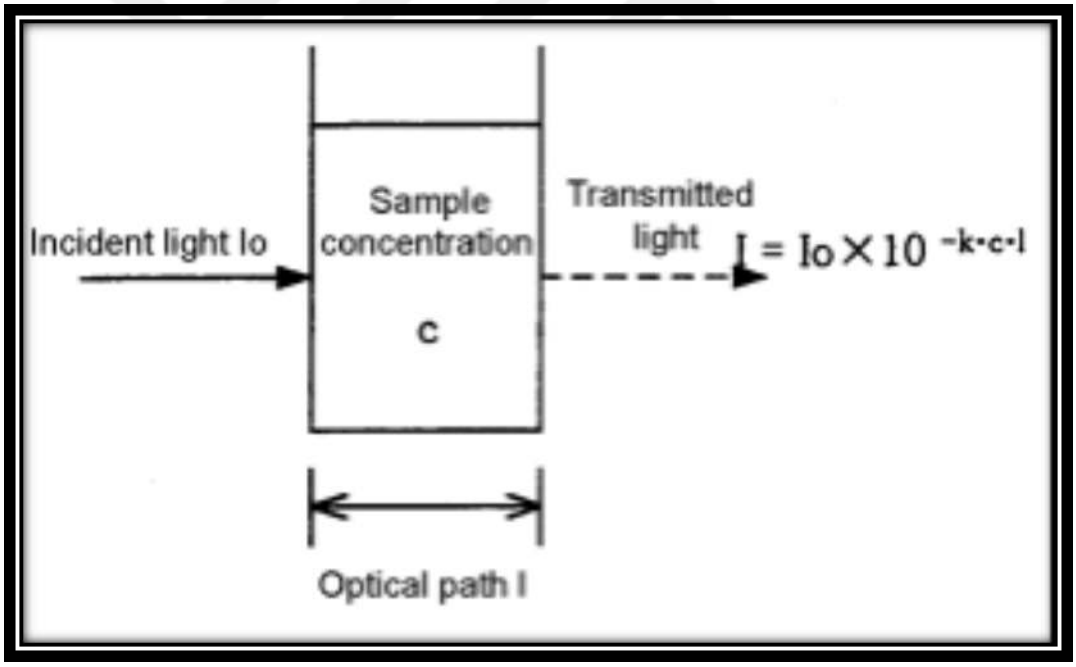

Figure 3.1 Lambert−Beer rule

Transmission (T) and absorption (A) is given by Equation (3.10) and Equation (3.11) (Verma and Mishra 2018).

$$T = \frac{I}{I_O} = 10^{-kcl} \tag{3.10}$$

$$A = \log\left(\frac{1}{T}\right) = \log(I/I_O) \quad (3.11)$$

Photons of UV-Visible light are capable of exciting solely the outer electrons from lower to higher energy levels. Due to the quantization of energy levels in matter, only the precise amount of light required to induce transitions between these states will be absorbed. Ultraviolet (UV) light is the sub-visible portion of the electromagnetic spectrum. The spectrum covers 100 to 400 nanometers. Several compounds may take in light of the visible or ultraviolet spectrum.

The energy absorption is normally associated with the moves of the electrons from the bonding orbitals to the anti-bonding orbitals. The difference in energy between these orbitals lies in the UV and Vis. range of the electromagnetic range. The relationship between the energy, denoted as E, of a single quantum and its frequency of oscillation, is proportional as in Equation (3.12).

$$E = h\nu = \frac{hc}{\lambda} \quad (3.12)$$

Where ν the frequency, λ is the related wavelength, and h is Plank's constant h=6.626x10^{-34} J.s.

When atoms within a molecule are excited electrically, they can spin and vibrate relative to one another. The energy levels of these rotations and vibrations are distinct from, but superimposed over, the electronic levels (Abdulsattar *et al.* 2014).

4. RESULTS AND DISCUSSION

Lopinavir (LOPV) (Pharmacopoeia 2007) is chemically known as (2S)-N-[(2S,4S,5S)-5-[2-(2,6-dimethylphenoxy) acetamido]-4-hydroxy-1,6-diphenylhexan-2-yl]-3-methyl-2-(2-oxo-1,3-diazinan-1-yl) butanamide and its empirical formula is $C_{37}H_{48}N_4O_5$ with a molecular weight of 628.80. LOPV is a drug approved by the FDA that serves as a protease inhibitor and is commonly used in the treatment of HIV patients. Lopinavir/ritonavir combination is used as a second line of protection in the treatment of HIV as recommended by The World Health Organization (WHO). Ritonavir aims to suppress the metabolic enzyme P450 3A and therefore improves the half-life of Lopinavir (Shaikh *et al.* 2020). This prevents cleavage of the gag-polyprotein and, therefore, improper viral assembly results. This subsequently results in non-infectious, immature viral particles. The chemical structure was shown in Figure 4.1. Literature review revealed that very few methods were reported for determining LOPV in bulk and pharmaceutical dosage form by UV spectrophotometric methods (Pharmacopoeia 2007, Seshachalam *et al.* 2007, Ponnilavarasan *et al.* 2010, Suneetha *et al.* 2011, WHO 2010).

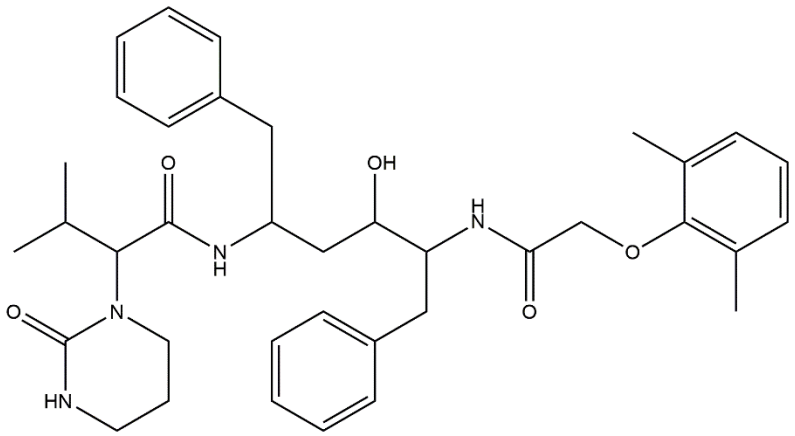

Figure 4.1 The chemical structure of the LOPV

Infectious Diseases Society of America (IDSA) guideline; has stated that clinical studies are needed to determine the use of LOPV for clinical study purposes only and to determine the place of LOPV and other HIV-1 protease inhibitors in the treatment of patients with COVID-19. Ministry of Health 11 March 2020 COVID-19 treatment in the directory; LOPV (2 x 400/100, 10-14 days) was recommended to be used in COVID-19

severe disease (Eroğlu *et al.* 2020). Available data suggest that for now, the role of LOPV in the treatment of COVID-19 is limited. In cases where it is used; It should be noted that the LOPV combination has serious drug interactions. Most common gastrointestinal and hepatotoxic side effects are observed (Furuta *et al.* 2013).

Many experimental studies have been conducted on the LOPV compound, which is used as a drug in the treatment of HIV, COVID-19, and viral diseases, and researchers have investigated how effective the LOPV compound is in the treatment of diseases. Although there are many experimental studies for the LOPV compound in the literature, few theoretical studies have been found. This thesis aims to obtain the molecular structure, bond parameters, molecular electrostatic potential map, and molecular orbital bond energies of the LOPV compound using the DFT method and to support the experimental UV-vis spectra in the literature with theoretical values. Single crystal structure and experimental bond parameters of the LOPV compound have not been found in the literature. Therefore, the experimental bond parameters of the Ritonavir compound, whose molecular structure is very similar, were compared with the theoretical values of the LOPV compound.

By choosing the DFT method, B3LYP base function, and 6-311G(d, p) and 6-311+G(d, p) basis sets, the molecular structure of the LOPV compound was optimized in ground state gas, ethanol, acetone, chloroform, and water environments. Then, single-point energy calculation was made with the same method using optimized structures. The theoretical UV-vis spectra of the LOPV compound were obtained for different solvent media using the TD-DFT method.

The (Crystallographic Information File) CIF containing the atomic coordinates of the compounds Ritonavir used to compare the bond parameters of the LOPV compound (CCDC number 710527) (Bauer *et al.* 2001) has been downloaded from the Cambridge Structural Database (Groom *et al.* 2016).

4.1 The Optimization Study of the LOPV Molecular Structure

LOPV compound with closed formula $C_{37}H_{48}N_4O_5$ consists of [2-(2,6-dimethylphenoxy) acetyl]amino], 4-hydroxy-1,6-diphenylhexan, and 3-methyl-2-(2-oxo-1,3-diazinan-1-yl) butanamide groups. Geometric optimization of the LOPV molecular structure was performed in both gaseous and solvent environments such as ethanol, acetone, chloroform, and water with different dielectric constant and polarity at the ground state by the DFT/B3LYP method and the 6-311G(d, p) and 6-311+G(d, p) basis sets (Table 4.1). The dielectric constants and dipole moments of the acetone, ethanol, chloroform, and water solvent are, μ=2.85 D, ε=20.7 μ=1.69 D, ε=24.5 μ=1.15 D, ε=4.81, and μ=1.82 D, ε=80.1, respectively. Polarity is influenced by the dielectric constant, which increases (in this study; water=high, gas phase=low). Another effect is the dipole moment. The optimized molecular structure of the LOPV is given in Figure 4.2.

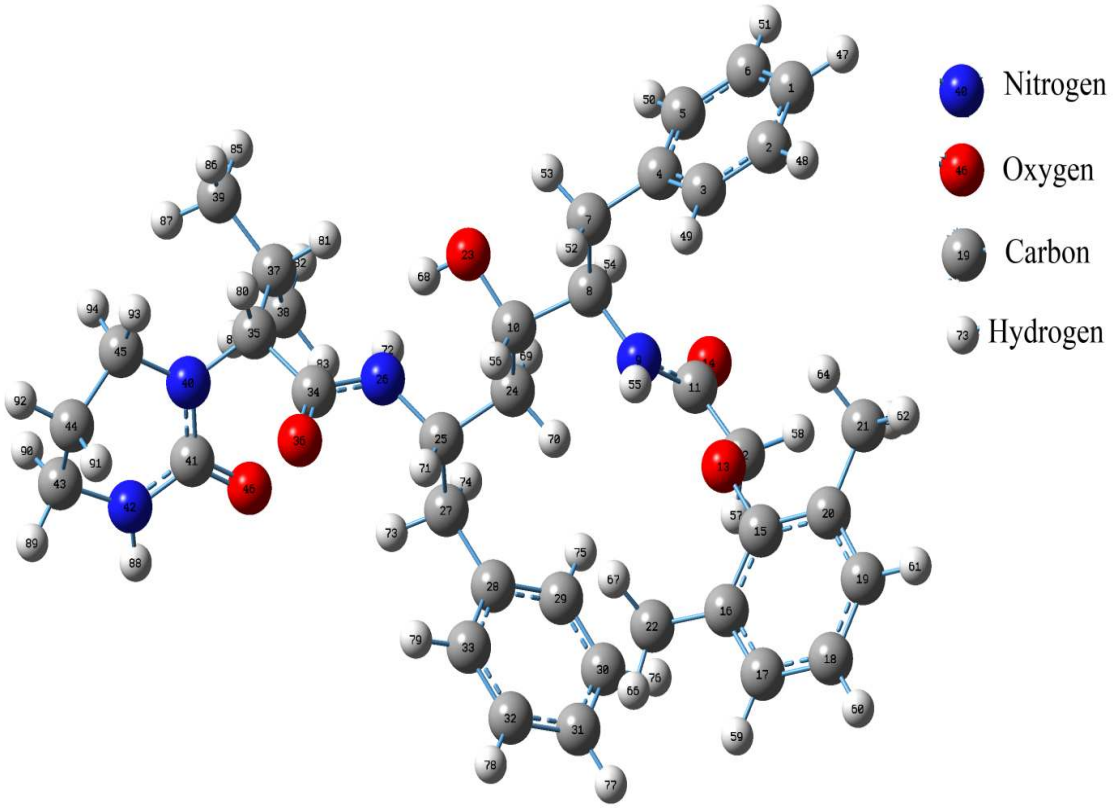

Figure 4.2 The optimized molecular structure of the LOPV by using DFT/B3LYP/6-311+G(d, p) in water media

Table 4.1 The theoretical bond parameters of the LOPV by using B3LYP/6-311G(d, p)

Lopinavir	B3LYP/6-311G(d, p) Water	B3LYP/6-311G(d, p) Acetone	B3LYP/6-311G(d, p) Chloroform	B3LYP/6-311G(d, p) Ethanol	B3LYP/6-311G(d, p) Gas
Bond lengths (Å)					
C1-C2	1.39372	1.39357	1.39319	1.39361	1.39239
C2-C3	1.39527	1.39523	1.39500	1.39524	1.39438
C3-C4	1.39923	1.39904	1.39863	1.39909	1.39804
C4-C5	1.40107	1.40101	1.40073	1.40102	1.40007
C5-C6	1.39331	1.39314	1.39268	1.39318	1.39183
C6-C1	1.39512	1.39508	1.39483	1.39509	1.39414
C4-C7	1.51227	1.51230	1.51225	1.51229	1.51207
C7-C8	1.54526	1.54499	1.54452	1.54506	1.54319
C8-N9	1.45904	1.45915	1.45911	1.45913	1.45892
N9-C11	1.34931	1.34978	1.35149	1.34967	1.35547
C11-O14	1.22748	1.22694	1.2250	1.22707	1.22061
C11-C12	1.52497	2.43635	1.52543	1.52505	1.52662
C12-O13	1.43032	1.43038	1.43062	1.43036	1.43097
O13-C15	1.39281	1.39272	1.39245	1.39273	1.39164
C15-C20	1.40157	1.40152	1.40134	1.40153	1.40112
C20-C19	1.39938	1.39932	1.39907	1.39934	139831
C19-C18	1.39136	1.39126	1.39090	1.39128	1.39023
C18-C17	1.39294	1.39290	1.39269	1.39291	1.39180
C17-C16	1.39745	1.39735	1.39703	1.39737	1.39652
C16-C22	1.50829	1.50829	1.50823	1.50829	1.50829
C8-C10	1.54576	1.54572	1.54547	1.54575	1.54524
C10-C24	1.53370	1.53355	1.53325	1.53358	1.53254
C24-C25	1.53503	1.53499	1.53495	1.53499	1.53404
C25-C27	1.55184	1.55170	1.55134	1.55175	1.55123
C27-C28	1.51224	1.51219	1.51210	1.51219	1.51191
C28-C29	1.39956	1.39952	1.39933	1.39952	1.39890
C29-C30	1.39525	1.39519	1.39495	1.39521	1.39433
C30-C31	1.39373	1.39369	1.39351	1.39370	1.39311
C31-C32	1.39542	1.39535	1.39514	1.39537	139455
C32-C33	1.39312	1.39306	1.39284	1.39306	1.39225
C33-C28	1.40167	1.40160	1.40141	1.40162	1.40092
C25-N26	1.47637	1.47664	1.47747	1.47659	1.47791
N26-C34	1.37137	1.37207	1.37415	1.37192	1.37569
C34-O36	1.22243	1.22188	1.22001	1.22201	1.21665
C34-C35	1.55097	1.55122	1.55210	1.55116	1.55362
C35-C37	1.55584	1.55589	1.55591	1.55587	1.55495
C37-C38	1.53587	1.53597	1.53615	1.53594	1.53614
C37-C39	1.53795	1.53798	1.53799	1.53798	1.53778
C35-N40	1.46639	1.46625	1.46601	1.46629	1.46651
N40-C45	1.47286	1.47244	1.47109	1.47255	1.46792
C45-C44	1.52453	1.52462	1.52492	1.52459	1.52582
C44-C43	1.52237	1.52248	1.52284	1.52246	1.52368
C43-N42	1.45965	1.45958	1.45901	1.45960	1.45814
N42-C41	1.36589	1.36615	1.36735	1.36609	1.37232
C41-O46	1.23802	1.23743	1.23524	1.23757	1.22924
C41-N40	1.37672	1.37705	1.23524	1.37697	1.38140
Bond angles (°)					
C1-C2-C3	120.14112	120.13444	120.121	120.136	120.087
C4-C5-C6	120.98938	120.98365	120.980	120.985	120.982
C6-C1-C2	119.48289	199.48300	119.480	119.483	119.479

Table 4.1 The theoretical bond parameters of the LOPV by using B3LYP/6-311G(d, p) (Continued)

Lopinavir	B3LYP/6-311G(d, p) Water	B3LYP/6-311G(d, p) Acetone	B3LYP/6-311G(d, p) Chloroform	B3LYP/6-311G(d, p) Ethanol	B3LYP/6-311G(d, p) Gas
C3-C4-C7	121.37891	121.35650	121.341	121.361	121.342
C5-C4-C7	120.37153	120.39262	120.416	120.388	120.457
C4-C7-C8	113.59653	113.65406	113.760	113.641	113.927
C7-C8-C10	111.70525	111.64271	111.502	111.656	111.262
C7-C8-N9	110.25190	110.25917	110.267	110.258	110.186
C8-N9-C11	124.17575	124.14530	124.022	124.155	123.635
N9-C11-O14	125.17167	125.19064	125.239	125.187	125.262
N9-C11-C12	115.47998	115.46473	115.390	115.470	115.183
O14-C11-C12	119.33724	119.33342	119.361	119.332	119.542
C11-C12-O13	110.96648	111.00650	111.072	110.998	111.096
C12-O13-C15	115.88593	115.85366	115.791	115.868	115.843
O13-C15-C20	119.54439	119.54302	119.534	119.551	119.420
C15-C20-C21	121.34981	121.34219	121.357	121.348	121.236
C15-C20-C19	117.71408	117.71509	117.727	117.714	121.236
C20-C19-C18	121.03709	121.03824	121.050	121.039	121.045
C19-C18-C17	119.99308	119.99188	119.974	119.992	119.958
C18-C17-C16	120.88168	120.88363	120.900	120.883	120.944
C17-C16-C22	121.39217	121.39963	121.413	121.399	121.388
O13-C15-C16	117.90928	117.91453	117.950	117.907	118.098
C15-C16-C22	120.69762	120.69075	120.675	120.690	120.716
C8-C10-O23	106.13956	106.18137	106.241	106.174	106.198
C8-C10-C24	112.36348	112.41115	112.499	112.401	112.428
O23-C10-C24	111.63921	111.62324	111.619	111.627	111.807
C10-C24-C25	114.98318	114.95776	114.917	114.965	115.077
C24-C25-N26	110.97751	110.98019	110.925	110.978	110.783
C24-C25-C27	112.34968	112.35439	112.372	112.357	112.193
C25-C27-C28	114.28447	114.24119	114.105	114.249	113.634
C27-C28-C29	121.54302	121.55704	121.577	121.556	121.618
C28-C29-C30	120.98362	120.98214	120.981	120.982	120.937
C29-C30-C31	120.13506	120.13430	120.133	120.135	120.150
C30-C31-C32	119.49948	119.49861	119.492	119.499	119.492
C31-C32-C33	120.15751	120.16197	120.180	120.161	120.189
C32-C33-C28	120.97090	120.96531	120.944	120.966	120.913
C33-C28-C27	120.20159	120.18356	120.152	120.185	120.064
C25-N26-C34	120.50396	120.42112	120.233	120.438	119.936
N26-C34-O36	122.37181	122.38772	122.494	122.385	122.855
N26-C34-C35	117.72780	117.71874	117.654	117.720	117.545
C34-C35-C37	118.48549	118.52276	118.617	118.517	118.907
C35-C37-C38	115.76973	115.77713	115.797	115.779	115.925
C35-C37-C39	110.19038	110.15512	110.079	110.160	109.894
C38-C37-C39	109.65683	109.64551	109.619	109.647	109.647
O36-C34-C35	119.48445	119.47619	119.424	119.478	119.191
C34-C35-N40	109.41985	109.40066	109.354	109.405	109.139
C37-C35-N40	115.16538	115.11950	115.035	115.128	115.027
C35-N40-N41	118.61407	118.53724	118.283	118.551	117.694
N40-C41-O46	121.92694	121.90908	121.890	121.912	122.086
C35-N40-C45	119.36930	119.41940	119.533	119.406	119.824
N40-C45-C44	110.99745	110.97644	110.961	110.982	110.833
C45-C44-C43	109.28514	109.28632	109.295	109.286	109.157

Table 4.1 The theoretical bond parameters of the LOPV by using B3LYP/6-311G(d, p) (Continued)

Lopinavir	**B3LYP/6-311G(d, p) Water**	**B3LYP/6-311G(d, p) Acetone**	**B3LYP/6-311G(d, p) Chloroform**	**B3LYP/6-311G(d, p) Ethanol**	**B3LYP/6-311G(d, p) Gas**
C44-C43-N42	108.75461	108.78561	108.883	108.787	109.093
C43-N42-C41	126.55699	126.55080	126.507	126.548	126.503
N42-C41-O46	120.80851	120.84902	120.942	120.840	120.978
Torsion angles (°)					
C3-C4-C7-C8	-100.26639	-101.44234	-103.322	-101.200	-104.774
C5-C4-C7-C8	79.31842	78.19734	76.366	78.426	75.032
C4-C7-C8-N9	64.22748	63.89876	63.447	63.968	62.838
C4-C7-C8-C10	-171.72850	-172.10111	-172.607	-172.021	-173.210
C7-C8-C10-O23	52.59698	52.57845	52.591	52.578	175.541
C7-C8-N9-C11	-126.50925	-127.15675	-128.239	-127.042	133.854
C8-N9-C11-O14	-5.91490	-6.04280	-6.572	-6.007	-7.520
O14-C11-C12-O13	169.72800	170.500064	172.343	170.382	174.020
N9-C11-C12-O13	-11.42200	-10.65440	-8.775	-10.767	-7.262
C11-C12-O13-C15	168.16733	168.59386	171.433	168.524	175.636
C12-O13-C15-C16	-99.38705	-99.3399-	-99.153	-99.391	-98.258
O13-C15-C16-C22	0.95018	0.95517	0.979	0.957	1.174
O13-C15-C20-C21	-1.52490	-1.051593	-1.506	-1.513	-1.607
C21-C20-C19-C18	179.10102	174.11138	179.100	179.107	179.072
O13-C15-C16-C17	-17783825	-177.8544	-177.846	-177.854	-177.698
O13-C15-C20-C19	177.71023	177.73428	177.744	177.734	177.638
C21-C20-C15-C16	-178.09874	-178.11573	-178.103	-178.109	-178.109
C22-C16-C15-C20	177.57727	177.60760	177.627	177.606	177.720
C22-C16-C17-C18	-178.49267	-178.52399	-178.562	-178.524	-178.659
C7-C8-C10-C24	174.88471	174.90321	175.004	174.897	175.541
O23-C10-C24-C25	-66.93660	-66.9593	-66.823	-66.944	-66.456
C10-C24-C25-C27	-71.24296	-71.26301	-171.551	-171.252	-171.623
C24-C25-C27-C28	70.32532	70.32150	70.195	70.321	70.010
C27-C28-C29-C30	-179.45004	-179.47460	-179.578	-179.471	179.966
C27-C28-C33-C32	179.53634	179.56977	179.716	179.565	-179.764
N26-C25-C27-C28	-165.7851	-156.76177	-165.908	-165.766	-166.141
C10-C24-C25-N26	-171.24296	56.55949	65.231	65.574	64.929
C24-C25-N26-C34	-153.14491	-153.0446	-152.812	-153.073	-154.428
C34-N26-C25-C27	82.15006	82.23875	82.450	82.211	80.408
C25-N26-C34-O36	61.25135	16.58352	17.071	16.520	16.061
C27-C25-N26-C34	82.15006	82.23875	82.450	82.211	80.408
O36-C34-C35-C37	175.96272	175.77128	174.911	175.826	174.711
C34-C35-C37-C38	76.70876	76.78536	77.130	76.758	76.821
C34-C35-C37-C39	-158.15503	-158.11803	-157.858	-158138	-158.184
C38-C37-C35-N40	-55.58214	-55.46370	-55.053	-55.502	-55.333
C39-C37-C35-N40	69.55407	69.63301	69.958	69.603	69.661
C37-C35-C34-O36	175.96272	175.77128	174.911	175.826	174.711
C39-C37-C35-C34	-158.15503	-158.1180-	-157.858	-158.138	-158.184
C37-C35-N40-C41	89.49893	89.55885	89.739	89.541	90.291
C37-C35-N40-C45	-97.45366	97.68599	-98.564	-97.660	-102.671
C35-N40-C41-O46	-4.89896	-5.03855	-5.520	-4.998	-8.986
C35-N40-C45-C44	-144.02733	-143.71383	-142.868	-143.792	-136.876
C35-N40-C41-N42	174.96908	174.44858	174.765	174.967	171.871
O46-C41-N40-C45	-177.78146	-177.62594	-177.033	-177.629	-175.842
O46-C41-N42-C43	174.42594	173.99211	172.977	174.073	168.419

The bond parameters including obtained bond lengths, bond angles, and torsion angles of the LOPV compound obtained from ground state optimized molecular structures for gas and different solvent environments using DFT/B3LYP/6-311G(d, p) and DFT/B3LYP/6-311+G(d, p) methods are given in Table 4.1 and Table 4.2, respectively.

Since the bond parameters of the molecular structure of the LOPV compound cannot be found in the literature, the bond parameters of the molecular structure of the Ritonavir compound, whose molecular structure is very similar, were compared in this thesis study.

[2-(2,6-dimethylphenoxy)acetyl]amino] group as group A, 4-hydroxy-1,6-diphenylhexane group as group B, and 3-methyl-2-(2-oxo-1,3-diazinan- 1-yl) butanamide group as group C in the LOPV compound were defined as seen in Figure 4.2. As seen in Table 4.1, C35(H)–N40 bond lengths in group C obtained by B3LYP/6-311G(d, p) method are 1.46639 Å (for water medium), 1.46625 Å (for acetone medium), 1.46601 Å (for chloroform medium), 1.46629 Å (for ethanol medium), and 1.46651 Å (for gas medium).

Table 4.2 The theoretical bond parameters of the LOPV by using B3LYP/6-311+G(d, p)

Lopinavir	**B3LYP/6-311+G(d, p) Water**	**B3LYP/6-311+G(d, p) Acetone**	**B3LYP/6-311+G(d, p) Chloroform**	**B3LYP/6-311+G(d, p) Ethanol**	**B3LYP/6-311+G(d, p) Gas**
Bond lengths (Å)					
C1-C2	1.39408	1.39397	1.39355	1.39400	1.39269
C2-C3	1.39608	1.39600	1.39576	1.39601	1.39513
C3-C4	1.39925	1.39914	1.39874	1.39916	1.39822
C4-C5	1.40181	1.40169	1.40137	1.40172	1.40069
C5-C6	1.39377	1.39363	1.39316	1.39366	1.39230
C6-C1	1.39614	1.39604	1.39572	1.39606	1.39500
C4-C7	1.51293	1.51290	1.51306	1.51290	1.51284
C7-C8	1.54574	1.54557	1.54447	1.54561	1.54319
C8-N9	1.46108	1.46102	1.54447	1.46103	1.46013
N9-C11	1.34678	1.34740	1.34949	1.34726	1.35478
C11-O14	1.23160	1.23089	1.22851	1.23105	1.22279
C11-C12	1.52444	1.52460	1.52524	1.52456	1.52645
C12-O13	1.42942	1.42962	1.43020	1.42957	1.43081
O13-C15	1.39383	1.39373	1.39324	1.39375	1.39217
C15-C20	1.40238	1.40235	1.40203	1.40236	1.40175
C20-C19	1.39997	1.39991	1.39972	1.39992	1.39087
C19-C18	1.39203	1.39193	1.39154	1.39195	1.39087
C18-C17	1.39342	1.39334	1.39320	1.39336	1.39087
C17-C16	1.39816	1.39808	1.39770	1.39809	1.39714

Table 4.2 The theoretical bond parameters of the LOPV by using B3LYP/6-311+G(d, p) (Continued)

Lopinavir	B3LYP/6-311+G(d, p) Water	B3LYP/6-311+G(d, p) Acetone	B3LYP/6-311+G(d, p) Chloroform	B3LYP/6-311+G(d, p) Ethanol	B3LYP/6-311+G(d, p) Gas
C16-C22	1.50802	1.50803	1.50810	1.50803	1.50829
C8-C10	1.54675	1.54672	1.54682	1.54673	1.54619
C10-C24	1.53407	1.53399	1.53327	1.53401	1.53268
C24-C25	1.53661	1.53656	1.53591	1.53657	1.53514
C25-C27	1.55130	1.55119	1.55113	1.55121	1.55085
C27-C28	1.51280	1.51278	1.51262	1.51279	1.51240
C28-C29	1.39972	1.39967	1.39949	1.39968	1.39908
C29-C30	1.39593	1.39586	1.39563	1.39588	1.39497
C30-C31	1.39411	1.39407	1.39379	1.39408	1.39334
C31-C32	1.39589	1.39583	1.39566	1.39585	1.39513
C32-C33	1.39367	1.39362	1.39354	1.39363	1.39294
C33-C28	1.40190	1.40186	1.40192	1.40187	1.40144
C25-N26	1.47775	1.47808	1.47936	1.47800	1.47929
N26-C34	1.36947	1.37036	1.37316	1.37015	1.37595
C34-O36	1.22514	1.22447	1.22247	1.22462	1.21801
C34-C35	1.55179	1.55208	1.55305	1.55202	1.55446
C35-C37	1.55672	1.55666	1.55644	1.55668	1.55585
C37-C38	1.53559	1.53564	1.53607	1.53563	1.53627
C37-C39	1.53852	1.53854	1.53855	1.53854	1.53837
C35-N40	1.46679	1.46669	1.46740	1.46671	1.46744
N40-C45	1.47526	1.47477	1.47308	1.47487	1.46941
C45-C44	1.52398	1.52409	1.52268	1.52406	1.52566
C44-C43	1.52179	1.52194	1.52268	1.52191	1.52360
C43-N42	1.46056	1.46054	1.45980	1.46056	1.45786
N42-C41	1.36673	1.36704	1.36804	1.36696	1.37287
C41-O46	1.24074	1.24001	1.23780	1.24019	1.23097
C41-N40	1.37502	1.37539	1.37600	1.37531	1.37941
Bond angles (°)					
C1-C2-C3	120.14104	120.13695	120.12616	120.13780	120.09602
C4-C5-C6	120.97840	120.97766	120.98209	120.97775	120.98838
C6-C1-C2	119.47182	119.47035	119.46026	119.47072	119.452994
C3-C4-C7	121.27690	121.28261	121.28569	121.28121	121.28792
C5-C4-C7	120.46092	120.45825	120.47751	120.45892	120.52629
C4-C7-C8	113.87499	113.91036	113.90067	113.90293	114.06593
C7-C8-C10	111.76132	111.71178	111.65510	111.72256	111.33186
C7-C8-N9	110.13567	110.13024	110.14858	110.13146	110.11869
C8-N9-C11	124.87329	124.83937	124.59215	124.84827	123.95982
N9-C11-O14	125.11361	125.12127	125.12992	125.11960	125.14279
N9-C11-C12	115.73022	115.70847	115.61395	115.71418	115.38120
O14-C11-C12	119.14975	119.16416	119.24879	119.16006	119.46324
C11-C12-O13	110.95873	110.99239	111.05362	110.98590	111.10321
C12-O13-C15	115.80177	115.79557	115.82326	115.79729	115.82943
O13-C15-C20	119.53718	119.54656	119.62246	119.54579	119.52079
C15-C20-C21	121.62607	121.62530	121.61813	121.62633	121.46357
C15-C20-C19	117.67012	117.67243	117.68189	117.67172	117.71625
C20-C19-C18	121.07662	121.08068	121.09687	121.08913	121.08440
C19-C18-C17	119.95882	119.95528	119.93755	119.95597	119.93008
C18-C17-C16	120.90872	120.91138	120.91656	120.91057	120.95072
C17-C16-C22	121.27528	121.26908	121.28184	121.27048	121.28639

Table 4.2 The theoretical bond parameters of the LOPV by using B3LYP/6-311+G(d, p) (Continued)

Lopinavir	B3LYP/6-311+G(d, p) Water	B3LYP/6-311+G(d, p) Acetone	B3LYP/6-311+G(d, p) Chloroform	B3LYP/6-311+G(d, p) Ethanol	B3LYP/6-311+G(d, p) Gas
O13-C15-C16	117.86876	117.86866	117.82188	117.86765	117.95741
C15-C16-C22	120.84219	120.84532	120.81534	120.84418	120.82389
C8-C10-O23	106.40796	106.43818	159.64178	106.43172	106.36075
C8-C10-C24	112.51291	112.55761	112.47975	112.54799	112.53742
O23-C10-C24	111.58292	111.55086	111.65619	111.55732	111.88963
C10-C24-C25	114.93426	114.90024	115.03424	114.90767	115.00954
C24-C25-N26	111.27888	111.28003	110.96828	111.28114	110.67856
C24-C25-C27	112.55450	112.57329	112.39775	112.57058	112.35152
C25-C27-C28	114.71229	114.66117	114.43516	114.67312	113.92091
C27-C28-C29	121.41597	121.43257	121.44980	121.42879	121.51683
C28-C29-C30	120.97185	120.97457	121.01016	120.97401	120.98433
C29-C30-C31	120.13725	120.13489	120.12777	120.13539	120.13821
C30-C31-C32	119.49677	119.49563	119.47893	119.49588	119.47782
C31-C32-C33	120.15327	120.15872	120.18745	120.15745	120.20006
C32-C33-C28	120.96748	120.96137	120.94994	120.96285	120.91826
C33-C28-C27	120.30450	120.28692	120.29979	120.29098	120.20210
C25-N26-C34	121.51195	121.37999	120.70197	121.40947	120.21023
N26-C34-O36	122.30337	122.32523	122.39906	122.32064	122.77357
N26-C34-C35	117.50543	117.53070	117.80808	117.52588	117.64998
C34-C35-C37	118.55322	118.57468	118.52169	118.56925	118.84916
C35-C37-C38	116.02102	116.00464	115.86484	116.00668	116.02704
C35-C37-C39	110.31679	110.29098	110.22967	110.29662	109.96511
C38-C37-C39	109.59656	109.58153	119.33965	109.58463	109.56218
O36-C34-C35	119.68846	119.63998	119.33965	119.64985	119.13340
C34-C35-N40	109.84532	109.80058	109.60156	109.80910	109.37702
C37-C35-N40	115.15881	115.13151	115.04846	115.13623	114.98936
C35-N40-N41	119.06519	118.97379	118.68242	118.99442	117.98923
N40-C41-O46	121.89197	121.87888	121.85520	121.88118	122.0516
C35-N40-C45	118.85537	118.94802	119.28163	118.93055	119.57724
N40-C45-C44	111.38363	111.34537	111.18123	111.35146	111.14327
C45-C44-C43	109.34128	109.34601	109.35074	108.69647	109.31186
C44-C43-N42	108.63917	108.70934	108.87352	109.34431	108.99695
C43-N42-C41	126.31263	126.34041	126.38686	126.33691	126.35883
N42-C41-O46	120.76486	120.80651	120.86282	120.79817	120.92742
Torsion angles (°)					
C3-C4-C7-C8	-105.24608	-105.53985	-107.58321	105.46804	-109.47381
C5-C4-C7-C8	74.93354	74.66236	72.51818	74.73041	-70.5748
C4-C7-C8-N9	64.11172	-172.52556	63.45610	64.14552	62.35072
C4-C7-C8-C10	-172.56647	-172.52556	-173.04927	172.53458	-173.97161
C7-C8-C10-O23	50.90226	51.01292	51.51722	50.98806	-52.29248
C7-C8-N9-C11	-123.33664	-124.17399	-127.40169	123.98872	-7.35281
C8-N9-C11-O14	-5.68384	-5.69981	-5.76578	5.69320	174.23062
O14-C11-C12-O13	172.37991	173.12589	174.11117	172.97824	-7.00281
N9-C11-C12-O13	-8.49436	-7.72681	-6.82392	7.87873	176.77457
C11-C12-O13-C15	176.07686	176.23821	174.37992	153.28269	-99.67356
C12-O13-C15-C16	-100.35894	-100.36492	-100.56399	100.37025	1.28394
O13-C15-C16-C22	1.30523	1.28725	1.15769	1.29304	-1.70775
O13-C15-C20-C21	-1.59785	-1.59025	-1.57202	1.59108	179.01237
C21-C20-C19-C18	178.90822	178.91501	178.92337	178.91242	179.01237

Table 4.2 The theoretical bond parameters of the LOPV by using B3LYP/6-311+G(d, p) (Continued)

Lopinavir	B3LYP/6-311+G(d, p) Water	B3LYP/6-311+G(d, p) Acetone	B3LYP/6-311+G(d, p) Chloroform	B3LYP/6-311+G(d, p) Ethanol	B3LYP/6-311+G(d, p) Gas
O13-C15-C16-C17	-177.77138	-177.78428	-177.80310	177.78131	-177.70516
O13-C15-C20-C19	177.73312	177.74516	177.73452	177.74243	177.63665
C21-C20-C15-C16	-177.79524	-177.80288	-177.78882	177.80008	-177.93578
C22-C16-C15-C20	177.56285	177.56022	177.43918	177.56246	177.56806
C22-C16-C17-C18	-178.69189	-178.68776	-178.56212	178.69048	-178.62544
C7-C8-C10-C24	173.39191	173.51063	174.13285	173.48352	175.14696
O23-C10-C24-C25	-68.80292	-68.77656	-66.93362	68.78639	-66.43739
C10-C24-C25-C27	-172.25574	-172.39043	-171.39560	172.36696	-170.58326
C24-C25-C27-C28	68.37644	68.44503	69.74362	68.43102	69.54706
C27-C28-C29-C30	-179.04349	-179.08564	-179.10599	179.07621	-179.63763
C27-C28-C33-C32	179.09704	179.14532	179.21593	197.13436	179.81501
N26-C25-C27-C28	-167.63808	-167.54311	-166.53027	176.56228	-166.77951
C10-C24-C25-N26	65.01316	64.83986	65.76963	64.87287	66.20187
C24-C25-N26-C34	-144.81153	-114.63361	-150.11565	144.66052	-153.18540
C34-N26-C25-C27	90.45232	90.59398	85.32016	90.57434	82.16921
C25-N26-C34-O36	16.33724	16.70398	17.87284	16.63875	16.49297
C27-C25-N26-C34	90.45232	90.59398	85.32016	90.57434	82.16921
O36-C34-C35-C37	178.91373	178.22345	173.90695	178.35930	173.39904
C34-C35-C37-C38	75.30618	75.54694	77.79810	75.50687	77.27670
C34-C35-C37-C39	-159.33210	-159.14725	-157.07585	157.17659	157.70486
C38-C37-C35-N40	-57.73952	-57.41876	-54.68909	57.47197	55.15168
C39-C37-C35-N40	67.62220	67.88705	70.43690	67.84458	69.86676
C37-C35-C34-O36	178.91373	178.22345	173.90695	178.35930	173.39904
C39-C37-C35-C34	-159.33210	-159.14725	-157.07585	159.17659	157.70486
C37-C35-N40-C41	88.02132	88.22038	88.95319	88.18623	89.22866
C37-C35-N40-C45	-96.97460	-97.16524	-97.08847	97.10622	100.73973
C35-N40-C41-O46	-2.32714	-2.51793	-3.00572	2.47246	5.93972
C35-N40-C45-C44	-148.16712	-147.62980	-146.19699	147.73764	142.12735
C35-N40-C41-N42	177.41715	177.39542	177.16561	177.40862	152.60949
O46-C41-N40-C45	-177.17364	-176.96933	-176.80810	177.01866	175.75335
O46-C41-N42-C43	176.60461	175.82661	174.05069	175.97317	171.71473

As seen in Table 4.2, C35(H)–N40 bond lengths in group C obtained by B3LYP/6-311+G(d, p) method are 1.46679 Å (for water medium), 1.46669 Å (for acetone medium), 1.46740 Å (for chloroform medium), 1.46671 Å (for ethanol medium), and 1.46744 Å (for gas medium).

The CH–N bond distance is listed as Gas> Water> Ethanol> Acetone> Chloroform obtained from the B3LYP/6-311G(d, p) method, while the bond distance obtained from the B3LYP/6-311+G(d, p) method is Gas> Chloroform > Water> Ethanol> Acetone.

In the literature, the CH–N bond distance from X-ray results was found to be 1.447(13) Å (Bauer *et al.* 2001). The closest experimental result for this bond distance was obtained from the chloroform medium by the B3LYP/6-311G(d, p) method (Figure 4.3).

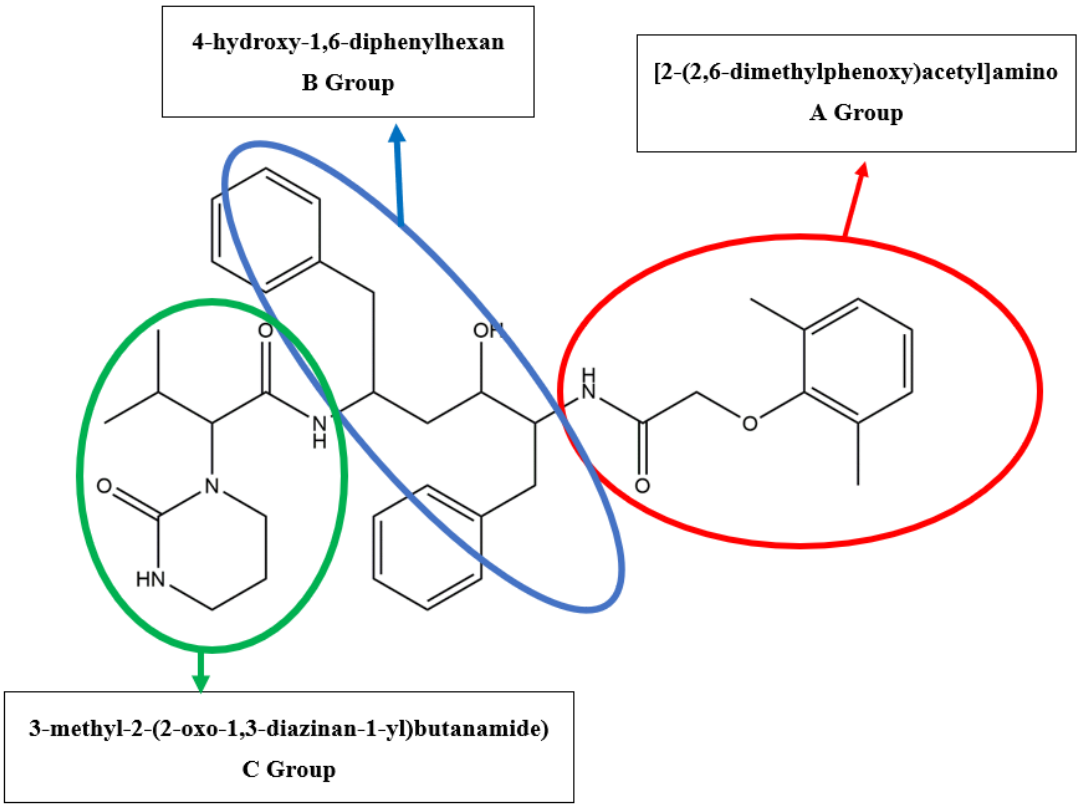

Figure 4.3 A, B, and C groups defined in the LOPV chemical structure

In group A of the LOPV, C11–N9(H) bond length obtained by the B3LYP/6-311G(d, p) method are 1.34931 Å (for water medium), 1.34978 Å (for acetone medium), 1.35149 Å (for chloroform medium), 1.34967 Å (for ethanol medium), and 1.35547 Å (for gas medium) while this length is 1.34678 Å (for water medium), 1.34740 Å (for acetone medium), 1.34949 Å (for chloroform medium), 1.34726 Å (for ethanol medium), and 1.35478 Å (for gas medium) by B3LYP/6-311+G(d, p) method. Also, in the group C of the LOPV, C34–N26(H) bond length obtained by B3LYP/6-311G(d, p) method are 1.37137 Å (for water medium), 1.37207 Å (for acetone medium), 1.37415 Å (for chloroform medium), 1.37192 Å (for ethanol medium), and 1.37569 Å (for gas medium) while this length is 1.36947 Å (for water medium), 1.37036 Å (for acetone medium),

1.37316 Å (for chloroform medium), 1.37015 Å (for ethanol medium), and 1.37595 Å (for gas medium) by B3LYP/6-311+G(d, p) method.

The C–NH bond distance is listed as Gas> Chloroform> Acetone> Ethanol> Water obtained from the B3LYP/6-311G(d, p) method, while the bond distance obtained from the B3LYP/6-311+G(d, p) method is Gas> Chloroform > Water> Acetone> Ethanol for the group A. For group C, the order is the same in both methods such as Gas> Chloroform> Acetone> Ethanol> Water.

In the literature, the C–NH bond distance from X-ray results was found to be 1.329(7) Å and 1.337(7) Å (Bauer *et al.* 2001). The closest experimental result for this bond distance was obtained from the water medium by the B3LYP/6-311G(d, p) method.

In group A of the LOPV, C12–O13 bond lengths obtained by the B3LYP/6-311G(d, p) method are 1.43032 Å (for water medium), 1.43038 Å (for acetone medium), 1.43062 Å (for chloroform medium), 1.43036 Å (for ethanol medium), and 1.43096 Å (for gas medium) while this length is 1.42942 Å (for water medium), 1.42962 Å (for acetone medium), 1.43020 Å (for chloroform medium), 1.42957 Å (for ethanol medium), and 1.43081 Å (for gas medium) by B3LYP/6-311+G(d, p) method.

The C–O bond distance is listed as Gas> Chloroform> Acetone> Ethanol> Water for B3LYP/6-311G(d, p) method and B3LYP/6-311+G(d, p) method.

In the literature, the C–O bond distance from X-ray results was found to be 1.429(6) Å (Bauer *et al.* 2001). The closest experimental result for this bond distance was obtained from the water medium by the B3LYP/6-311+G(d, p) method.

In group A of the LOPV, C11=O34 bond length obtained by B3LYP/6-311G(d, p) method are 1.22748 Å (for water medium), 1.22694 Å (for acetone medium), 1.2250 Å (for chloroform medium), 1.22707 Å (for ethanol medium), and 1.22061 Å (for gas medium) while this length is 1.23160Å (for water medium), 1.23089 Å (for acetone

medium), 1.22851 Å (for chloroform medium), 1.23105 Å (for ethanol medium), and 1.22279 Å (for gas medium) by B3LYP/6-311+G(d, p) method. Also, in the group C of the LOPV, C34=O36 bond length obtained by the B3LYP/6-311G(d, p) method are 1.22243 Å (for water medium), 1.22188 Å (for acetone medium), 1.22001 Å (for chloroform medium), 1.22201 Å (for ethanol medium), and 1.21665 Å (for gas medium) while this length is 1.22514 Å (for water medium), 1.22447 Å (for acetone medium), 1.22247 Å (for chloroform medium), 1.22462 Å (for ethanol medium), and 1.21801 Å (for gas medium) by B3LYP/6-311+G(d, p) method.

The C=O bond distance is listed as Water> Ethanol> Acetone> Chloroform> Gas for B3LYP/6-311G(d, p) method and B3LYP/6-311+G(d, p) method.

In the literature, the C=O bond distance from X-ray results was found to be 1.241(6) Å, 1.227(9) Å, and 1.219(6) Å (Bauer *et al.* 2001). The closest experimental result for this bond distance was obtained from the water and ethanol medium by the B3LYP/6-311G(d, p) method and B3LYP/6-311+G(d, p) method.

4.2 The Energy Study of the LOPV Molecular Structure

The total energy of the LOPV molecular structure was calculated in ground state DFT/B3LYP/6-311G(d, p) and DFT/B3LYP/6-311+G(d, p) in both gaseous and acetone, chloroform, ethanol, and water environments. One of the parameters that indicate the stability of a molecule is its total energy. According to the calculated environments, the total energy of the LOPV molecular structure can be given as Gas> Chloroform> Acetone> Ethanol> Water for both methods from large to small. The lowest energy structure of the LOPV molecular structure was obtained from the water environment; the total energy of the LOPV molecular structure corresponding to the lowest energy is -2034.6346 a.u. by using B3LYP/6-311+G(d, p). The total energy values of the LOPV molecular structure are given in Table 4.3 and Table 4.4. The highest dipole moment of the LOPV molecular structure can be listed as Gas> Acetone> Ethanol> Chloroform> Water for both methods. Total energy and dipole moment values of the LOPV molecular

structure were found to be similar to different methods in the literature (Makhlouf *et al.* 2023).

Frontier molecular orbitals (FMOs) have an important role in the understanding of organic reaction mechanisms and the analysis of drug-receptor interactions (Makhlouf *et al.* 2023). FMOs of the LOPV are calculated by using DFT/B3LYP/6-311G(d, p) and DFT/B3LYP/6-311+G(d, p) in both gaseous and acetone, chloroform, ethanol, and water environments. The most important FMOs in a molecule are the HOMO, which is the highest molecular orbital occupied by electrons and capable of donating one electron, and the LUMO, which is the lowest molecular orbital unoccupied by electrons, capable of accepting one electron. The narrower the $E_{HOMO}(E_H)$-$E_{LUMO}(E_L)$ gap (ΔE) of a molecule, the softer and chemically reactive the molecule, and the wider the ΔE, the harder and kinetically stable the molecule. The order of the ΔE can be given as Gas> Chloroform> Acetone> Ethanol> Water for both methods. The narrow ΔE value (6.0239 eV) of LOPV in the water environment indicates that the structure is softer in this environment compared to other environments. As seen in Figure 4.4, π electrons in π-bonding molecular orbitals are delocalized on the 2-oxo-1,3-diazinan group. However, if the π^*-anti-bonding molecules are the π^* electrons in the orbitals, it is seen that the LOPV is delocalized in the phenyl ring in group B. The calculated Density of State (DOS) spectrum of the LOPV molecular structure is given in Figure 4.4. The calculated HOMO and LUMO energy values of the LOPV molecular structure are given in Table 4.3 and Table 4.4. When the HOMO and LUMO energy values calculated for different methods and environments of the LOPV molecular structure in the literature are examined, it is seen that they are compatible with the values found in this thesis study (Flores-Holguín and Glossman-Mitnik 2020). From the E_H and E_L values, the global reactivity parameters of the molecular structures can be derived as follows.

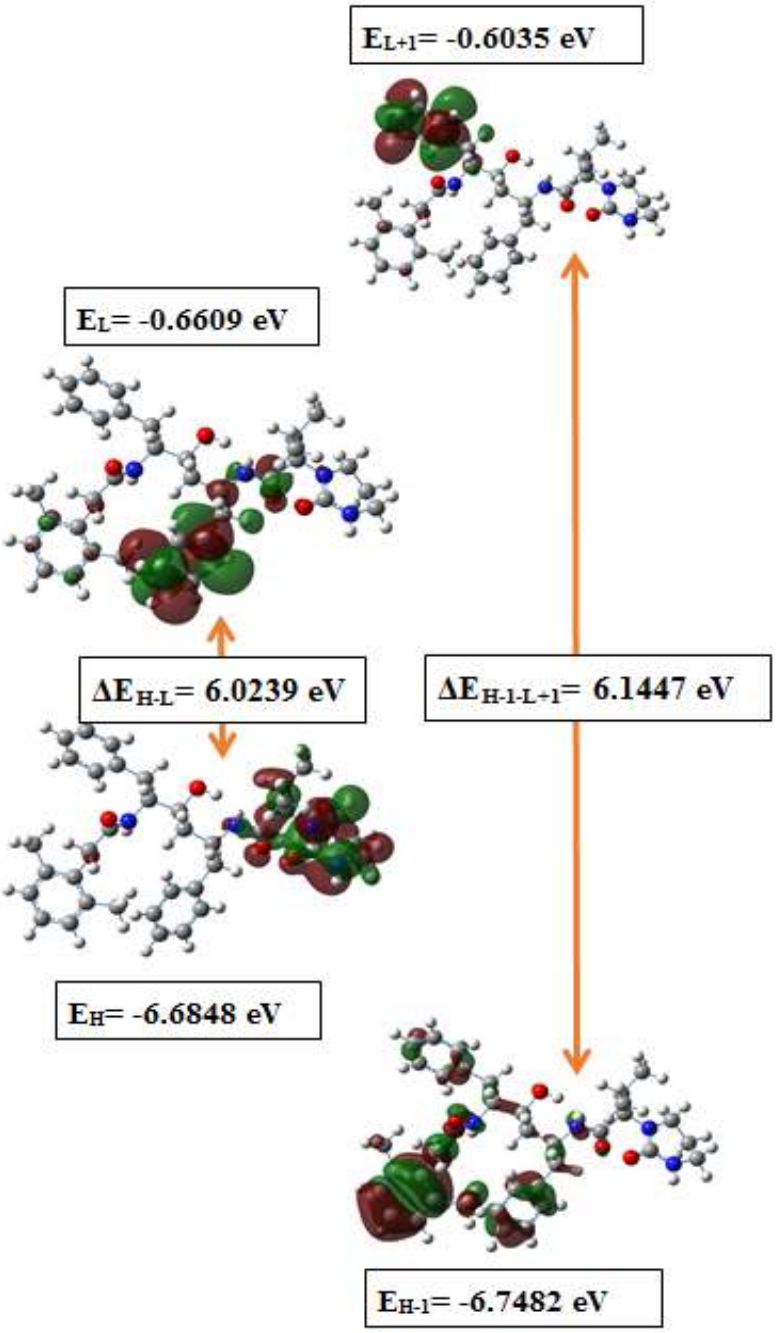

Figure 4.4 The molecular orbital energies of the LOPV by using B3LYP/6-311+G(d, p) in water media

The ionization potential (IP) is the lowest energy required to remove an electron from a molecule. The term "electron affinity" (EA) refers to the energy that a molecule obtains when it accepts an extra electron. Electronegativity (χ) is a measure of an atom's ability to attract shared electrons to itself. The chemical potential (μ_{CP}) represents the tendency for an electron to escape from a system in equilibrium. It is equal to minus the

electronegativity. The chemical hardness (η) measures a molecule's resistance to intramolecular charge transfer. The stabilizing energy when a system receives an additional electronic charge from the outside environment is indicated by the electrophilicity index (ω), which is defined in terms of the square of chemical potential divided by the chemical hardness. The global softness (S) is inversely proportional to chemical hardness (Pearson 1997). These parameters of the LOPV are defined as Equation (4.1), Equation (4.2), Equation (4.3), Equation (4.4), Equation (4.5), Equation (4.6), and Equation (4.7);

$$IP = -E_H \tag{4.1}$$

$$EA = -E_L \tag{4.2}$$

$$\chi = \frac{(IP+EA)}{2} \tag{4.3}$$

$$\mu_{CP} = -\chi \tag{4.4}$$

$$\eta = \frac{(IP-EA)}{2} \tag{4.5}$$

$$\omega = \frac{\mu^2}{2\eta} \tag{4.6}$$

$$S = \frac{1}{2\eta} \tag{4.7}$$

The ionization potentials of the LOPV vary from 6.4273 to 6.6848 eV. The greater facility to form a cation is for B3LYP/6-311+G(d, p) method and water media. The electronic affinities of the LOPV vary from 0.2334 to 0.6609 eV. The greater facility to form an anion is for B3LYP/6-311+G(d, p) method and water media. Chemical Hardness values range from 3.0119 to 3.0969 eV. This means that the LOPV in water media with 3.0119 eV has the lowest resistance to change its electronic configuration; thus, it will react more

easily in the presence of the protease. Electronegativity values are located between 3.3303 and 3.6728 eV. A bigger tendency to attract electrons in LOPV is found in water, ethanol, and acetone respectively (Figure 4.5).

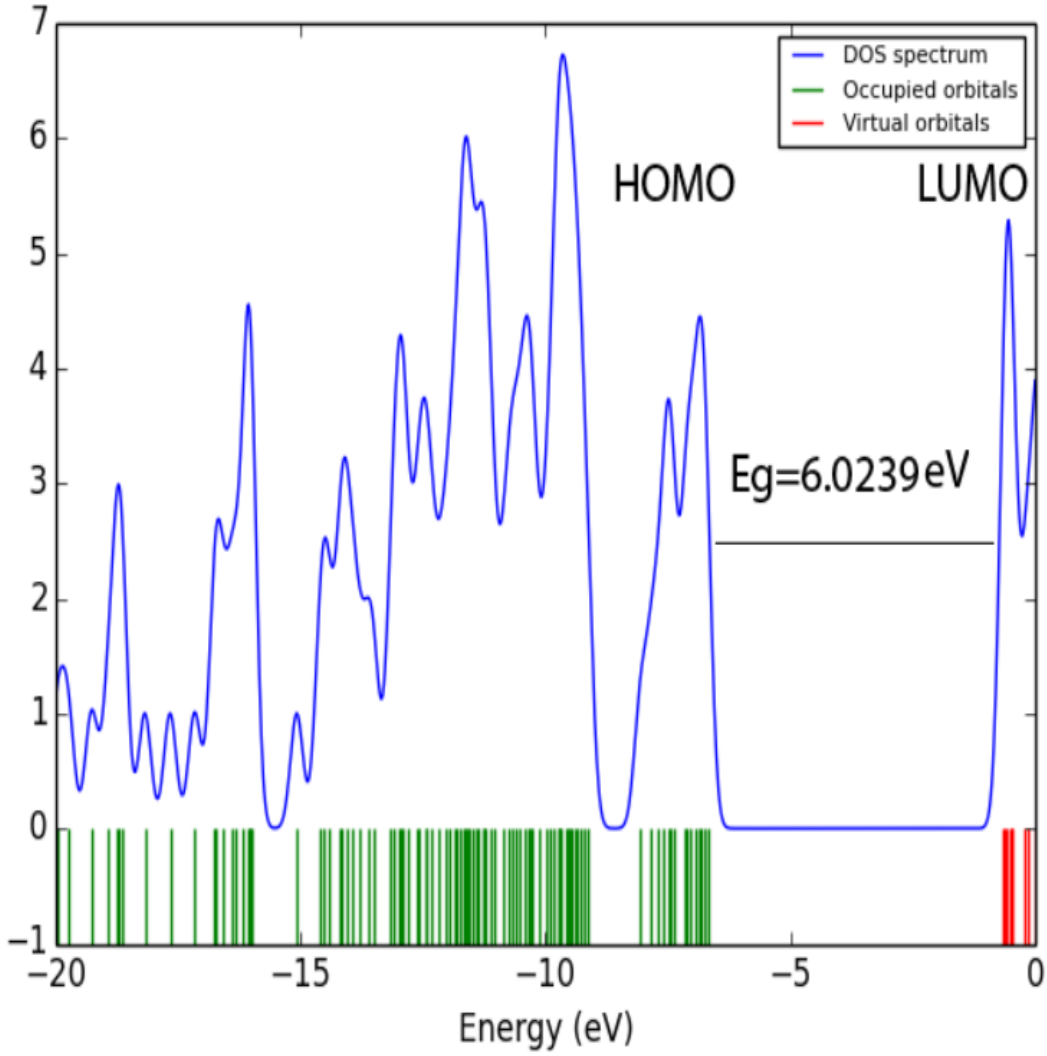

Figure 4.5 The Density of States spectrum of the LOPV by using B3LYP/6-311+G(d, p) in water media

The Electrophilicity values are in a range of 1.7906 to 2.2393 eV. This property denotes the capacity to stabilize the energy of a system when it becomes saturated with electrons from the surroundings. The LOPV which is most capable to stabilize energy is found in water media.

Figure 4.6 is given the calculated molecular orbital energy levels of LOPV molecular structure in water media and the percentage contributions of functional groups to these energy levels by the B3LYP/6-311+G(d, p) method. The contribution of the LOPV molecular structure to the HOMO energy level is 81% from group C, 18% from group B and 1% from group A, while the LUMO energy level is contributed by 56% from group B, 22% from group C and 21% from group A. It can be seen in Figure 4.6, Table 4.3, and Table 4.4.

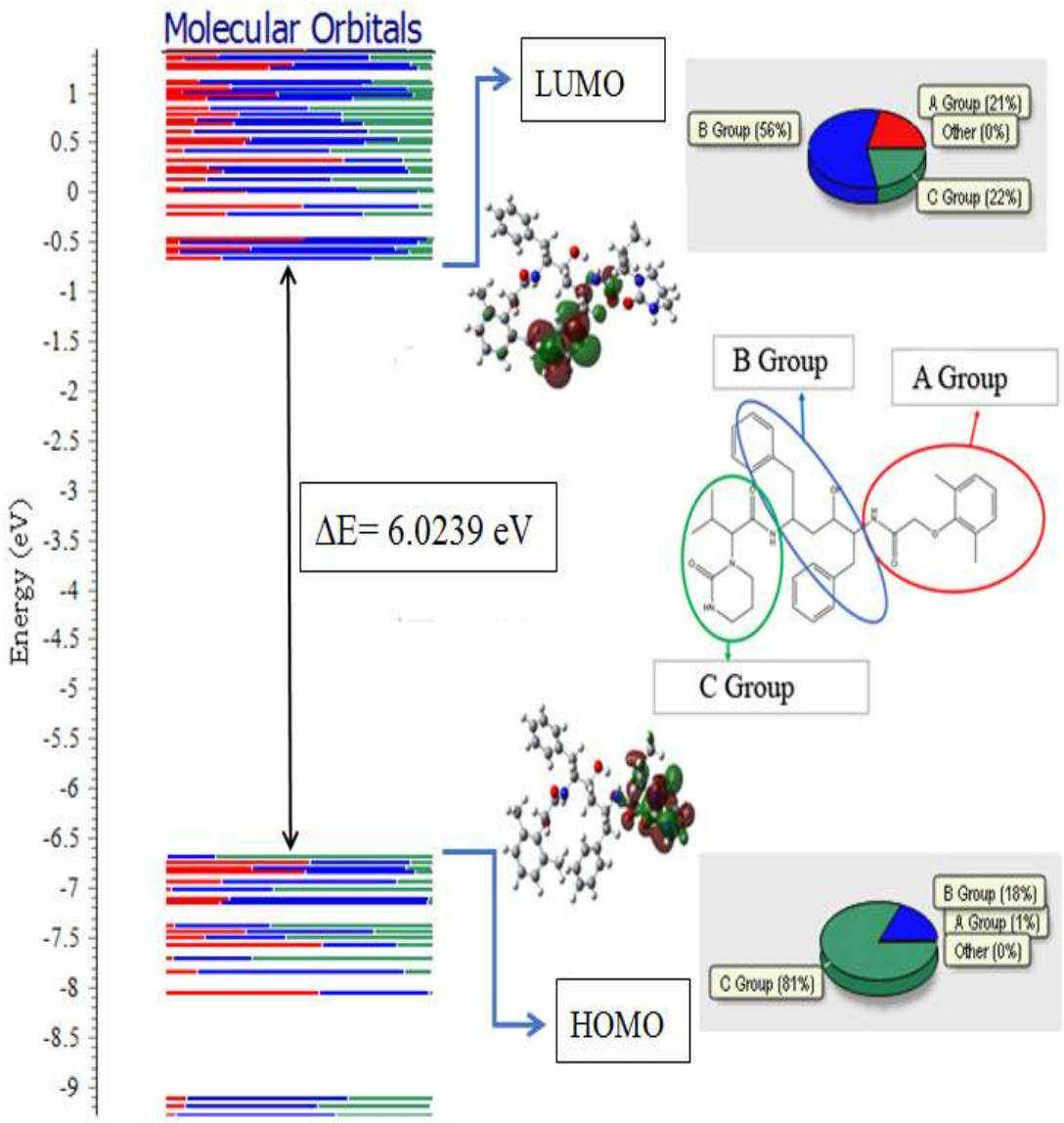

Figure 4.6 The calculated molecular orbital energy levels of LOPV molecular structure in water media and the percentage contributions of functional groups to these energy levels with by B3LYP/6-311+G(d, p) method

Table 4.3 The molecular orbital energy values, total energies, dipole moment values, and the global reactivity of the LOPV obtained by using the DFT/B3LYP/6-311G(d, p) method

Lopinavir	**6-311G (d, p) Gas**	**6-311G (d, p) Ethanol**	**6-311G (d, p) Chloroform**	**6-311G (d, p) Acetone**	**6-311G (d, p) Water**
$\mathbf{E_H(eV)}$	6.4273	6.5424	6.5302	6.5416	6.5449
$\mathbf{E_L(eV)}$	0.2334	0.4664	0.3891	0.4620	0.4813
ΔE (eV)	6.1939	6.0760	6.1411	6.0796	6.0636
Total energy (a.u)	-2034.5741	-2034.6011	-2034.5932	-2034.6007	-2034.6027
Dipole Moment (Debye)	6.2189	6.1418	5.8744	6.1560	4.7302
IP (eV)	6.4273	6.5424	6.5302	6.5416	6.5449
EA (eV)	0.2334	0.4664	0.3891	0.4620	0.4813
$\boldsymbol{\mu_{CP}}$ **(eV)**	-3.3303	-3.5044	-3.4596	-3.5018	-3.5131
χ (eV)	3.3303	3.5044	3.4596	3.5018	3.5131
S (eV^{-1})	0.1614	0.1645	0.1628	0.1644	0.1649
η (eV)	3.0969	3.038	3.0705	3.0398	3.0318
ω (eV)	1.7906	2.0212	1.9489	2.0170	2.0353

Table 4.4 The molecular orbital energy values, total energies, dipole moment values, and the global reactivity of the LOPV obtained by using the DFT/B3LYP/6-311+G(d, p) method

Lopinavir	**6-311+G (d, p) Gas**	**6-311+G (d, p) Ethanol**	**6-311+G (d, p) Chloroform**	**6-311+G (d, p) Acetone**	**6-311+G (d, p) Water**
$\mathbf{E_H(eV)}$	6.5373	6.6807	6.6559	6.6796	6.6848
$\mathbf{E_L(eV)}$	0.4557	0.6462	0.5665	0.6419	0.6609
ΔE (eV)	6.0816	6.0345	6.0894	6.0377	6.0239
Total energy (a.u)	-2034.6029	-2034.6328	-2034.6240	-2034.6323	-2034.6346
Dipole Moment (Debye)	6.4105	6.3404	6.0360	6.3576	4.9150
IP (eV)	6.5373	6.6807	6.6559	6.6796	6.6848
EA (eV)	0.4557	0.6462	0.5665	0.6419	0.6609
$\boldsymbol{\mu_{CP}}$ **(eV)**	-3.4965	-3.6634	-3.6112	-3.6607	-3.6728
χ (eV)	3.4965	3.6634	3.6112	3.6607	3.6728
S (eV^{-1})	0.1644	0.1657	0.1642	0.1656	0.1660
η (eV)	3.0408	3.0172	3.0447	3.0188	3.0119
ω (eV)	2.0102	2.2239	2.1415	2.2195	2.2393

4.3 The Molecular Electrostatic Potential Map of the LOPV Molecular Structure

A molecular electrostatic potential (MEP) map of the LOPV molecular structure was obtained by DFT/BLYP/6-311+G(d, p) method in the ground state water environment. The MEP map of the LOPV molecular structure was calculated to identify the electron-

rich and electron-poor regions in the molecular structure. The blue region on the potential energy surface of the LOPV molecular structure in Figure 4.7 represents the electron-poor electrophilic region, and the red region represents the electron-rich nucleophilic region. As seen from the potential energy surface of LOPV, a nucleophilic region was formed on the oxygen atoms in the A, B, and C groups, and an electrophilic region was formed on the protons attached to the nitrogen atom in the A and C groups.

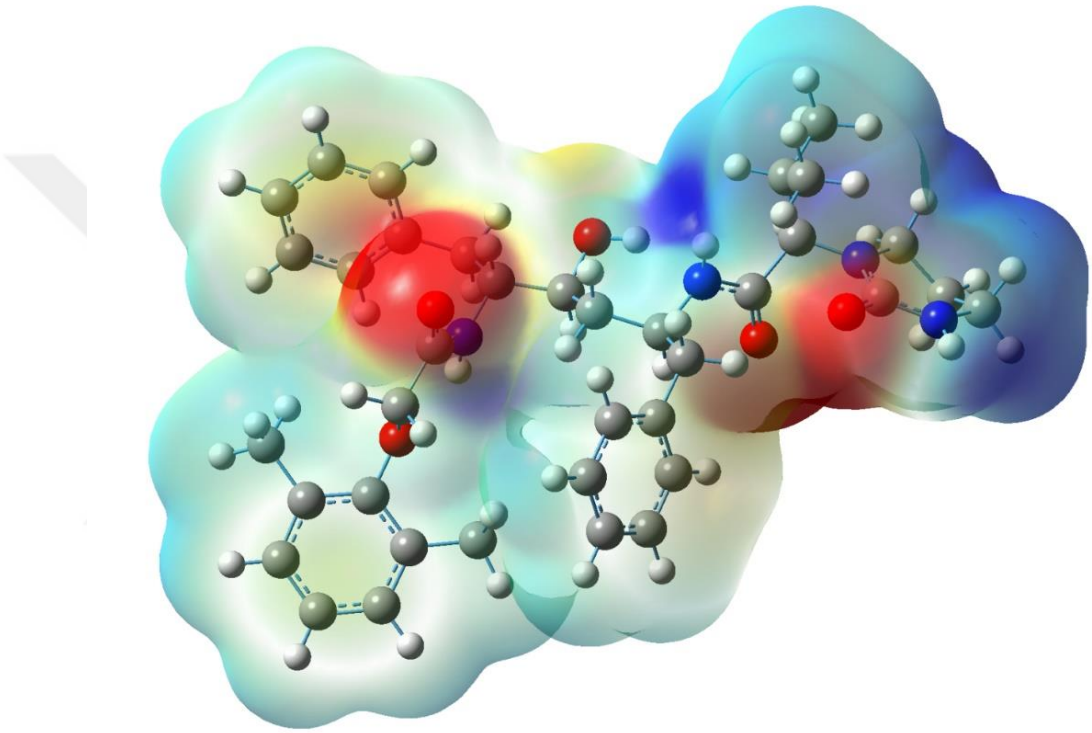

Figure 4.7 The molecular electrostatic potential map of the LOPV

4.4 The UV-Vis Spectra Study of the LOPV Molecular Structure

The theoretical UV-vis spectra of the LOPV molecular structure were obtained by the TD-DFT/B3LYP/6-311G(d, p) and TD-DFT/B3LYP/6-311+G(d, p) methods. Solvents with different dielectric constants and dipole moments were included in the calculations to investigate the effect of different solvent environments on absorption wavelengths in the UV-vis spectra of the LOPV molecular structure. UV-vis spectra of molecular structures, electron density distributions, and functional to molecular orbitals The contribution calculation of the groups made with the Chemissian package program. The

theoretical UV-vis spectra of the LOPV molecular structure obtained in the gas, ethanol, acetone, chloroform, and water media by B3LYP/6-311+G(d, p) are given in APPENDIX 1, APPENDIX 2, APPENDIX 3, APPENDIX 4, and APPENDIX 5, respectively.

Experimental UV spectra studies for the LOPV drug in the literature have reported that the LOPV drug absorbs at a wavelength in the range of 255-264 nm (Salunke *et al.* 2013, Sangshetti *et al.* 2014, Jadhav *et al.* 2018).

Figure 4.8 and Figure 4.9 show the UV-vis spectra of the LOPV molecular structure calculated in gas and solvent environments. As seen in Table 4.5, Figure 4.8, and Figure 4.9, the solvent we can say that the UV-vis spectra obtained in the gas environment shift to lower energy-high wavelengths compared to the gas environment. In other words, lower energy is needed in the solvent medium for absorption to take place. As can be seen from Table 4.5, it is seen that the molecular structure of LOPV absorbs in the wavelength range of 211-220 nm. According to the B3LYP/6-311+G(d, p) method, the LOPV molecular structure was absorbed in lower energy compared to the other method.

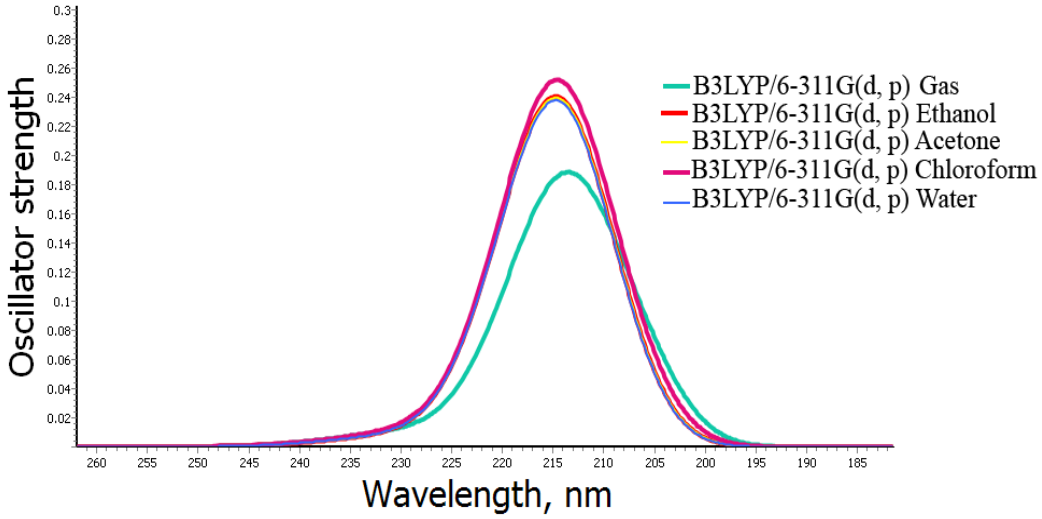

Figure 4.8 UV-vis spectra of LOPV molecular structure calculated by TD-DFT/B3LYP/6-311G(d, p) method in different solvent environments

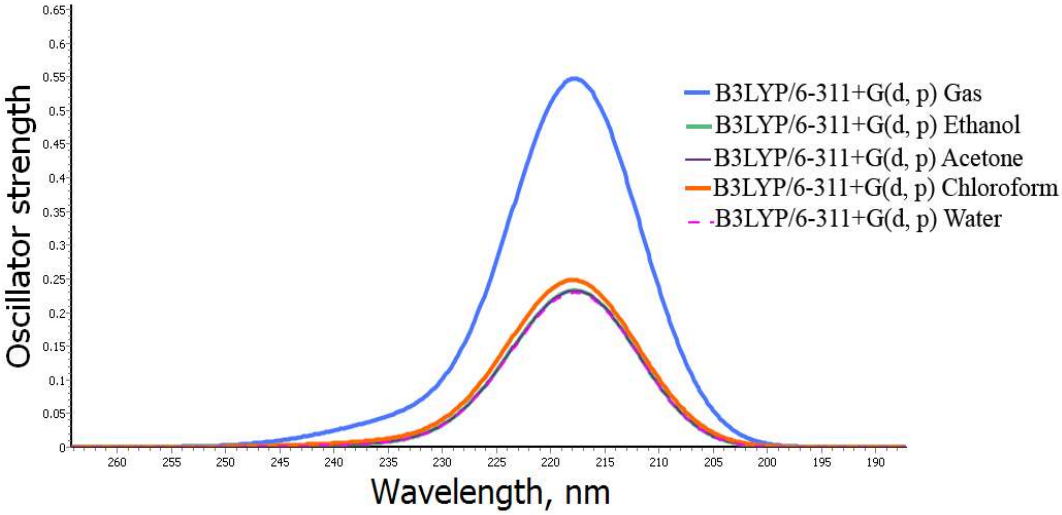

Figure 4.9 UV-vis spectra of LOPV molecular structure calculated by TD-DFT/B3LYP/6-311+G(d, p) method in different solvent environments

Table 4.5 Transitions of molecular orbital energy levels (for 20 states), percent distributions, absorption wavelengths, and oscillator stresses of the Lopinavir compound (f) (168. MO HOMO-1: H-1, 169. MO HOMO: H, 170. MO LUMO: L, and 171. MO LUMO+1: L+1)

TD-DFT	Wavelengths(nm) (% Distr.)	f	MO→MO	TD-DFT	Wavelengths(nm) (% Distr.)	f	MO→MO
6-311G (d, p) Gas	215(62%) 213(20%) 206(56%)	0.107 0.025 0.011	H→L H→L+1 H-2→L+1	**6-311+G (d, p) Gas**	219(66%) 216(58%)	0.114 0.035	H→L H→L+1
6-311G (d, p) Ethanol	216(47%) 212(17%) 211(36%)	0.145 0.029 0.015	H-1→L H-1→L+2 H→L+1	**6-311+G (d, p) Ethanol**	220(17%) 218(32%) 215(37%)	0.079 0.060 0.037	H-1→L H-1→L H-2→L+1
6-311G (d, p) Acetone	216(47%) 212(18%) 210(38%)	0.146 0.029 0.014	H-1→L H-1→L+2 H→L+1	**6-311+G (d, p) Acetone**	220(17%) 218(30%) 215(40%)	0.080 0.061 0.037	H-1→L H-1→L H-2→L+1
6-311G (d, p) Chloroform	216(33%) 212(15%) 211(59%)	0.138 0.028 0.012	H→L H→L+2 H-2→L+1	**6-311+G (d, p) Chloroform**	219(29%) 215(24%)	0.123 0.042	H-1→L H→L+1
6-311G (d, p) Water	216(46%) 213(56%) 211(24%)	0.135 0.023 0.021	H-1→L H-1→L+1 H-2→L+1	**6-311+G (d, p) Water**	220(16%) 218(39%) 215(29%)	0.075 0.054 0.032	H→L H-1→L H-2→L+1

5. CONCLUSIONS AND RECOMMENDATION

5.1 Conclusion

- It was found that some of the bond parameters of the molecular structure of the LOPV compound optimized by the B3LYP/6-311G(d, p) method were shorter than the bond parameters of the molecular structure optimized by the B3LYP/6-311+G(d, p) method. The same is true and vice versa.
- When the bond parameters in the optimized molecular structure of the LOPV compound were compared with the experimental bond parameters in the literature, it was found that the bond parameters mostly obtained from the water environment were compatible with the more experimental values.
- The molecular structure of LOPV was found to be at the lowest energy at –2034.6346 a.u., in the water environment by the B3LYP/6-311+G(d, p) method.
- It was found that the total energy values of the LOPV molecular structure obtained by the B3LYP/6-311+G(d, p) method were lower than the total energy values obtained from the B3LYP/6-311G(d, p) method.
- According to the total energy values obtained, it can be said that the molecular structure of LOPV is more stable in the water environment.
- The narrow ΔE value of LOPV in the water environment indicates that the structure is softer in this environment compared to other environments.
- According to the HOMO-LUMO range, we can say that the molecular structure of LOPV is chemically active in the water environment compared to other environments.
- Considering the percentage contribution of the LOPV molecular structure to the molecular orbitals, it is seen that the highest contribution to the HOMO energy level of the LOPV molecular structure is from the electrons of the atoms in the 3-methyl-2-(2-oxo-1,3-diazinan-1-yl) butanamide functional group. We can say that the contribution of its structure to the LUMO energy level comes mostly from the electrons of the atoms in the 4-hydroxy-1,6-diphenylhexane functional group.
- The molecular electrostatic potential map of the LOPV molecular structure shows that the N-H group will be a donor group due to an electrophilic feature of the molecular

structure in any intermolecular interaction, and oxygen atoms will be the acceptor group due to its nucleophilic feature.

- It can be said that the molecular structure of LOPV absorbs theoretically in the wavelength range of 211-220 nm.
- To absorb the LOPV molecular structure, lower energy is needed in the solvent environment than in the gaseous environment.

5.2 Recommendation

- UV-vis spectra of the LOPV molecular structure can also be obtained and compared in other solvent environments.
- Contributions to the molecular orbital energy levels of the LOPV molecular structure can be obtained from which orbital of which atom contributes.

REFERENCES

Abdulsattar, M. A., Hussein, M. T. and Hameed, H. A. 2014. Ab initio structural and vibrational properties of GaAs diamondoids and nanocrystals. AIP Advances, 4(12): 127119.

Artika, I. M., Dewantari, A. K. and Wiyatno, A. 2020. Molecular biology of coronaviruses: current knowledge. Heliyon, 6(8): e04743.

Azadparvar, M., Kheirabadi, M. and Aliabad, H. R. 2022. Fluorinated derivatives of tetrahydroaltersolanol molecule on COVID-19, HIV, and HTLV protease by DFT and molecular docking approaches. Journal of Molecular Modeling, 28(11): 350.

Bauer, J., Spanton, S., Henry, R., Quick, J., Dziki, W., Porter, W. and Morris, J. 2001. Ritonavir: an extraordinary example of conformational polymorphism. Pharmaceutical Research, 18: 859-866.

Becke, A. 1993. Density-functional thermochemistry. III. The role of exact Exchange. The Journal of Chemical Physics, 98: 5648.

Bransden, B. H. and Joachain, C. J. 2003. Physics of atoms and molecules. Pearson Education India, 1114 page, Noida.

Chitturi, S. R., Bharathi, C., Reddy, A. R., Reddy, K. C., Sharma, H. K., Handa, V. K. and Bindu, V. H. 2008. Impurity profile study of lopinavir and validation of HPLC method for the determination of related substances in lopinavir drug substance. Journal of Pharmaceutical and Biomedical Analysis, 48(5): 1430-1440.

Containing, K. E. H. 2020. 2019-nCoV (Wuhan) coronavirus. Health Care Management Science, 23(3): 311-314.

Cramer, C. J. 2013. Essentials of computational chemistry: theories and models. John Wiley & Sons, 624 page, New York.

Cutnell, J. D., Johnson, K. W., Young, D. and Stadler, S. 2021. Physics. John Wiley & Sons, 1120 page, New York.

Czech, B., Krzyszczak, A., Boguszewska-Czubara, A., Opielak, G., Jośko, I. and Hojamberdiev, M. 2022. Revealing the toxicity of lopinavir-and ritonavir-containing water and wastewater treated by photo-induced processes to Danio rerio and Allivibrio fischeri. Science of the Total Environment, 824: 153967.

Donato, E. M. 2008. Lopinavir/ritonavir cápsulas: perfil de dissolução in vitro baseado nos dados in vivo, estudos de estabilidade térmica e metodologia analítica. Journal of Pharmaceutical and Biomedical Analysis, 47: 542-547.

Donato, E. M., Dias, C. L., Rossi, R. C., Valente, R. S., Fröehlich, P. E. and Bergold, A. M. 2006. LC method for studies on the stability of lopinavir and ritonavir in soft gelatin capsules. Chromatographia, 63: 437-443.

Dorsett, H. and White, A. 2000. Overview of molecular modelling and ab initio molecular orbital methods suitable for use with energetic materials. Defence Science and Technology Laboratory, 1-8.

Eroğlu, E., Tarakçı, A., Çölkesen, F., Şengöz, M., Kacar, F. and Özdemir, Ş. 2020. COVID-19 Hastalarında lopinavir/ritonavir ve favipravir deneyimi. Journal of Contemporary Medicine, 10(4): 642-646.

Fermi, E. 1927. Un metodo statistico per la determinazione di alcune priorieta dell'atome. The Accademia dei Lincei, 6(32): 602-607.

Fitts, D. D. 1999. Principles of quantum mechanics: as applied to chemistry and chemical physics. Cambridge University Press, 351 page, Cambridge.

Flores-Holguín, N. and Glossman-Mitnik, D. 2020. Molecular Docking and conceptual DFT-based study of some potential SARS-CoV-2 inhibitors. Computational Molecular Bioscience, 10(04): 111.

Fock, V. 1930. Näherungsmethode zur Lösung des quantenmechanischen Mehrkörperproblems. Zeitschrift für Physik, 61: 126-148.

Frisch, M. J., Trucks, G. W., Schlegel, H. B., Scuseria, G. E., Robb, M. A., Cheeseman, J. R. and Fox, D. J. 2009. Gaussian 09 Revision A. 1. Gaussian Incorporated, 139.

Furuta, Y., Gowen, B. B., Takahashi, K., Shiraki, K., Smee, D. F. and Barnard, D. L. 2013. Favipiravir (T-705), a novel viral RNA polymerase inhibitor. Antiviral Research, 100(2): 446-454.

Gandhimathi, R., Vijayaraj, S. and Jyothirmaie, M. P. 2012. Analytical process of drugs by ultraviolet (UV) spectroscopy–a review. International Journal of Pharmaceutical Research & Analysis, 2(2): 72-78.

Gorbalenya, A. E., Baker, S. C., Baric, R. S., de Groot, R. J., Drosten, C., Gulyaeva, A. A. and Ziebuhr, J. 2020. The species Severe acute respiratory syndrome-related

coronavirus: classifying 2019-nCoV and naming it SARS-CoV-2. Nature Microbiology, 5(4): 536-544.

Gorbalenya, A. E., Enjuanes, L., Ziebuhr, J. and Snijder, E. J. 2006. Nidovirales: evolving the largest RNA virus genome. Virus Research, 117(1): 17-37.

Gotwals, R. R. and Sendlinger, S. C. 2007. A chemistry educator's guide to molecular modeling. Journal of the North Carolina School of Science and Mathematics. 1-9.

Grant, W. B. 2002. An estimate of premature cancer mortality in the US due to inadequate doses of solar ultraviolet-B radiation. Cancer, 94(6): 1867-1875.

Groom, C. R., Bruno, I. J., Lightfoot, M. P. and Ward, S. C. 2016. The Cambridge structural database. Acta Crystallographica Section B: Structural Science, Crystal Engineering and Materials, 72(2): 171-179.

Guideline, I. H. T. 2005. Validation of analytical procedures: Text and methodology. Q2 (R1), 1(20): 5.

Heidari, A. 2020. Investigation of prevention, protection and treatment of Ritonavir effectiveness on coronavirus disease–2019 (COVID–19) infection using fourier transform raman (FT–Raman) biospectroscopy. Saudi Journal of Biomedical Research, 5(7): 212-235.

Hohenberg, P. and Kohn, W. 1964. Inhomogeneous electron gas. Physical Review, 136(3): 864.

Hu, Q., Xiong, Y., Zhu, G. H., Zhang, Y. N., Zhang, Y. W., Huang, P. and Ge, G. B. 2022. The SARS-CoV-2 main protease (Mpro): Structure, function, and emerging therapies for COVID-19. MedComm, 3(3): e151.

Hutter, J. 2005. Lecture notes in computational chemistry electronic structure theory. Physical Chemistry Institute, University of Zurich, Winter Thurerstrasse, 190: 8057.

Jadhav, S. R., Alhat, H. P. and Joshi, S. 2018. Analytical methods development & validation for simultaneous estimation of Lopinavir & Ritonavir in pharmaceutical formulation by simultaneous equation method using Uv spectrophotometry. International Research Journal of Pharmacy, 9(8).

Jones, R. O. 2006. Introduction to density functional theory and exchange-correlation energy functionals. Computational Nanoscience: Do It Yourself, 31: 45-70.

Kampen, H. M., Méndez, H. and Zahn, D. R. T. 1999. Energy level alignment at molecular semiconductor/GaAs (100) Interaces: where is the LUMO. University of Chemnitz, Institut fur Germany, 28.

Ketterer, B., Heiss, M., Uccelli, E., Arbiol, J. and Fontcuberta i Morral, A. 2011. Untangling the electronic band structure of wurtzite GaAs nanowires by resonant Raman spectroscopy. ACS Nano, 5(9): 7585-7592.

Koch, W. and Holthausen, M. C. 2015. A chemist's guide to density functional theory. John Wiley & Sons, 313 page, New York.

Kohanoff, J. and Gidopoulos, N. I. 2003. Density functional theory: basics, new trends and applications. Handbook of Molecular Physics and Quantum Chemistry, 2(5): 532-568.

Kohn, W. and Sham, L. J. 1965. Self-consistent equations including exchange and correlation effects. Physical Review, 140(4): 1133.

Kwon, O., Coropceanu, V., Gruhn, N. E., Durivage, J. C., Laquindanum, J. G., Katz, H. E. and Brédas, J. L. 2004. Characterization of the molecular parameters determining charge transport in anthradithiophene. The Journal of Chemical Physics, 120(17): 8186-8194.

Lee, C., Yang, W. and Parr, R. G. 1988. Development of the Colle-Salvetti correlation-energy formula into a functional of the electron density. Physical Review B, 37(2): 785.

Lipkowitz, K. B. and Boyd, D. B. 2009. Reviews in computational chemistry. John Wiley & Sons, 560 page, New York.

Lippi, G., Simundic, A. M. and Plebani, M. 2020. Potential preanalytical and analytical vulnerabilities in the laboratory diagnosis of coronavirus disease 2019 (COVID-19). Clinical Chemistry and Laboratory Medicine, 58(7): 1070-1076.

Makhloufi, A., Ghemit, R., El Kolli, M. and Baitiche, M. 2023. Computational investigation into Nirematrelvir/Ritonavir synergetic efficiency compared with some approved antiviral drugs targeting main protease (Mpro) SARS-CoV-2 Omicron variant. Journal of the Indian Chemical Society, 100(3): 100891.

Minkin, V. I. 1999. Glossary of terms used in theoretical organic chemistry. Pure and Applied Chemistry, 71(10): 1919-1981.

Mirza, M. U. and Froeyen, M. 2020. Structural elucidation of SARS-CoV-2 vital proteins: Computational methods reveal potential drug candidates against main protease, Nsp12 polymerase and Nsp13 helicase. Journal of Pharmaceutical Analysis, 10(4): 320-328.

Mueller, M. R. 2007. Fundamentals of quantum chemistry: molecular spectroscopy and modern electronic structure computations. Springer Science & Business Media, 265 page, Berlin.

Nelson, C. W. 2020. COVID-19: time for WHO to reconsider its stance towards Taiwan. Nature, 579(7798): 193-194.

Parr, R. G. and Yang, W. 1995. Density-functional theory of the electronic structure of molecules. Annual Review of Physical Chemistry, 46(1): 701-728.

Pavia, D. L., Lampman, G. M., Kriz, G. S. and Vyvyan, J. A. 2014. Introduction to spectroscopy. Cengage learning, 784 page, Boston.

Pearson, R. G. 1997. Chemical hardness. Wiley, 210 page, Weinheim.

Pharmacopoeia, I. 2007. Government of India, the Indian Pharmacopoeia Commission. Ministry Of Health And Family Welfare, 1174.

Ponnilavarasan, I., Rajasekaran, A., Dharuman, J. G., Kalaiyarasi, D. and Senthilkumar, M. 2010. RP–HPLC method for simultaneous estimation of antiretroviral drugs lopinavir and ritonavir in tablet dosage form. Digest Journal of Nanomaterials and Biostructures, 5(3): 771-8.

Raj, V. S., Mou, H., Smits, S. L., Dekkers, D. H., Müller, M. A., Dijkman, R. and Haagmans, B. L. 2013. Dipeptidyl peptidase 4 is a functional receptor for the emerging human coronavirus-EMC. Nature, 495(7440): 251-254.

Reimers, J. R. 2011. Computational methods for large systems: electronic structure approaches for biotechnology and nanotechnology. John Wiley & Sons, 688 page, New York.

Rogers, D. W. 2003. Computational chemistry using the PC. John Wiley & Sons, 349 page, New York.

Sadasivam, K. and Kumaresan, R. 2011. Theoretical investigation on the antioxidant behavior of chrysoeriol and hispidulin flavonoid compounds–A DFT study. Computational and Theoretical Chemistry, 963(1): 227-235.

Salunke, J. M., Pawar, D. S., Chavhan, V. D. and Ghante, M. R. 2013. Simultaneous UV spectrophotometric method for estimation of ritonavir and lopinavir in bulk and tablet dosage form. Scholars Research Library, 5(3): 156-162.

Sangshetti, N. J., Bhojane, S., Rashid, S. B. and Gonjari, I. 2014. Spectrophotometric method for simultaneous estimation of lopinavir and ritonavir in bulk and tablet dosage form. International Journal of ChemTech Research, 6: 823-827.

Santos, J. C., Andres, J., Aizman, A. and Fuentealba, P. 2005. An aromaticity scale based on the topological analysis of the electron localization function including σ and π contributions. Journal of Chemical Theory and Computation, 1(1): 83-86.

Seshachalam, U., Haribabu, B. and Chandrasekhar, K. B. 2007. A novel validated LC method for quantitation of lopinavir in bulk drug and pharmaceutical formulation in the presence of its potential impurities and degradation products. Biomedical Chromatography, 21(7): 716-723.

Shaikh, V. S., Shaikh, Y. I. and Ahmed, K. 2020. A molecular docking study of lopinavir towards SARS-COV-2 target protein. Engineered Science, 12(2): 113-116.

Sherrill, C. D. 2002. Introduction to electronic structure theory. The Journal of Chemical Physics, 1-8.

Sholl, D. S. and Steckel, J. A. 2011. Density functional theory: a practical introduction. John Wiley & Sons, 256 page, New York.

Springborg, M. 2000. Methods of electronic-structure calculations: from molecules to solids. Reports on Progress in Physics, 75(3): 036503.

Suneetha, A., Kathirvel, S. and Ramachandrika, G. 2011. A validated RP HPLC method for simultaneous estimation of lopinavir and ritonavir in combined dosage form. International journal of Pharmacy and Pharmaceutical Sciences, 3(1): 49-51.

Thakkar, H. and Patel, K. 2010. A first-derivative spectrophotometric method for the estimation of Lopinavir in tablets. Chronicles of Young Scientists, 1(3): 22-22.

Thomas, L. H. 1927. The calculation of atomic fields. In Mathematical proceedings of the Cambridge philosophical society. Cambridge University Press, 23(5): 542-548.

Valone, S. M. 2010. Quantal density functional theory II. Approximation Methods and Applications, 132(32): 11387-11388.

Verma, G. and Mishra, M. 2018. Development and optimization of UV-Vis spectroscopy-a review. World Journal of Pharmaceutical Research, 7(11): 1170-1180.

WHO, World Health Organization. 2010. Antiretroviral therapy for HIV infection in adults and adolescents: recommendations for a public health approach-2010 revision. World Health Organization, 2010.

Yang, J. S., Chiang, J. H., Tsai, S. C., Hsu, Y. M., Bau, D. T., Lee, K. H. and Tsai, F. J. 2020. In silico de novo curcuminoid derivatives from the compound library of natural products research laboratories inhibit COVID-19 3CLpro activity. Natural Product Communications, 15(9): 1934578X20953262.

Young, D. 2004. Computational chemistry: a practical guide for applying techniques to real world problems. John Wiley & Sons, 408 page, New York.

Yüksektepe, Ç. 2009. Bazı imidazol, tiyazol ve schiff bazlı bileşiklerin kristal yapılarının x-ışını ve hesaplamalı yöntemlerle belirlenmesi. PhD. Thesis, Ondokuz Mayıs Üniversitesi, 151 page, Samsun.

Zhao, W. M., Song, S. H., Chen, M. L., Zou, D., Ma, L. N., Ma, Y. K. and Bao, Y. M. 2020. The 2019 novel coronavirus resource. Hereditas, 42(2): 212-221.

APPENDICES

APPENDIX 1. UV-vis spectra of LOPV molecular structure obtained by B3LYP/6-311+G(d, p) method in gas environment

APPENDIX 2. UV-vis spectra of LOPV molecular structure obtained by B3LYP/6-311+G(d, p) method in ethanol environment

APPENDIX 3. UV-vis spectra of LOPV molecular structure obtained by B3LYP/6-311+G(d, p) method in acetone environment

APPENDIX 4. UV-vis spectra of LOPV molecular structure obtained by B3LYP/6-311+G(d, p) method in chloroform environment

APPENDIX 5. UV-vis spectra of LOPV molecular structure obtained by B3LYP/6-311+G(d, p) method in water environment

APPENDIX 1. UV-vis spectra of LOPV molecular structure obtained by B3LYP/6-311+G(d, p) method in gas environment

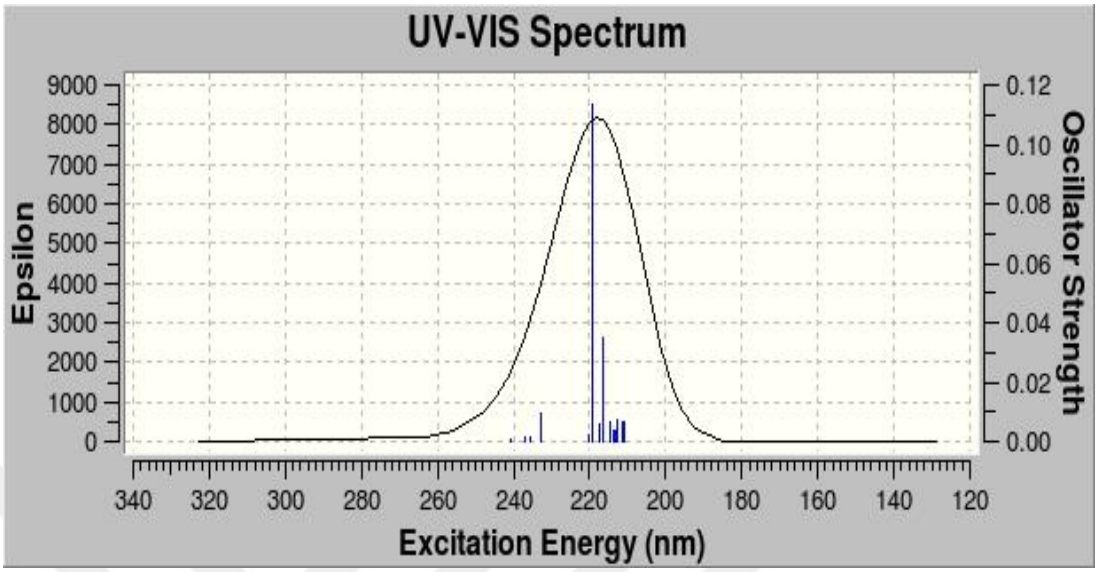

APPENDIX 2. UV-vis spectra of LOPV molecular structure obtained by B3LYP/6-311+G(d, p) method in ethanol environment

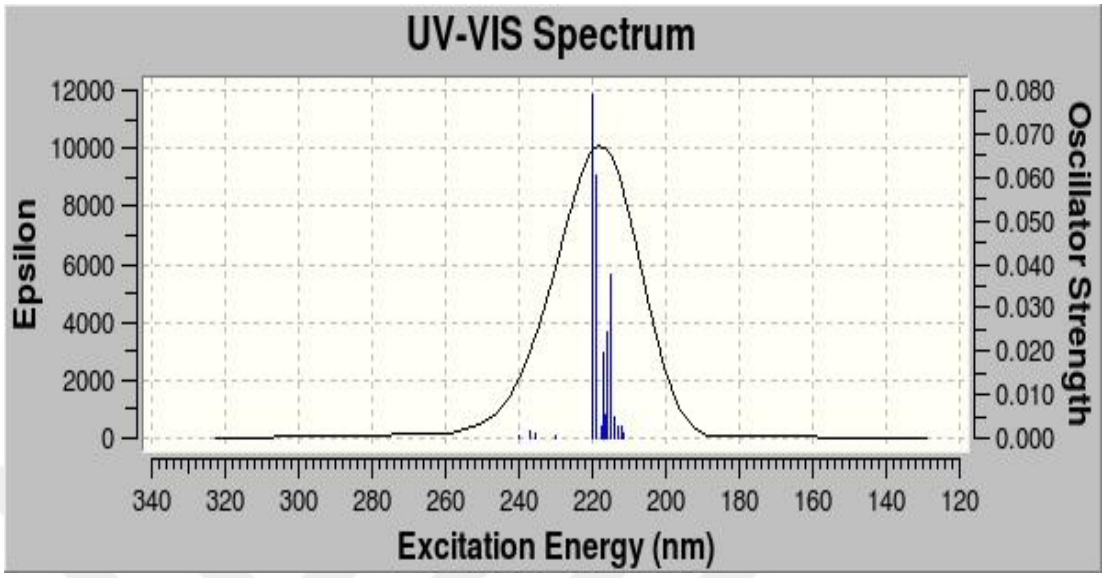

APPENDIX 3. UV-vis spectra of LOPV molecular structure obtained by B3LYP/6-311+G(d, p) method in acetone environment

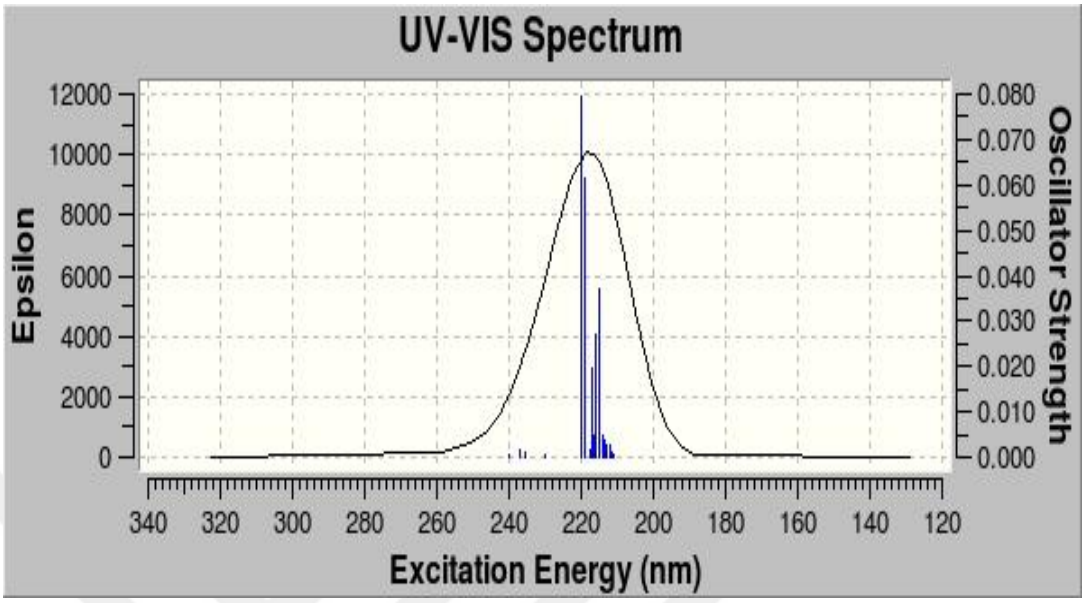

APPENDIX 4. UV-vis spectra of LOPV molecular structure obtained by B3LYP/6-311+G(d, p) method in chloroform environment

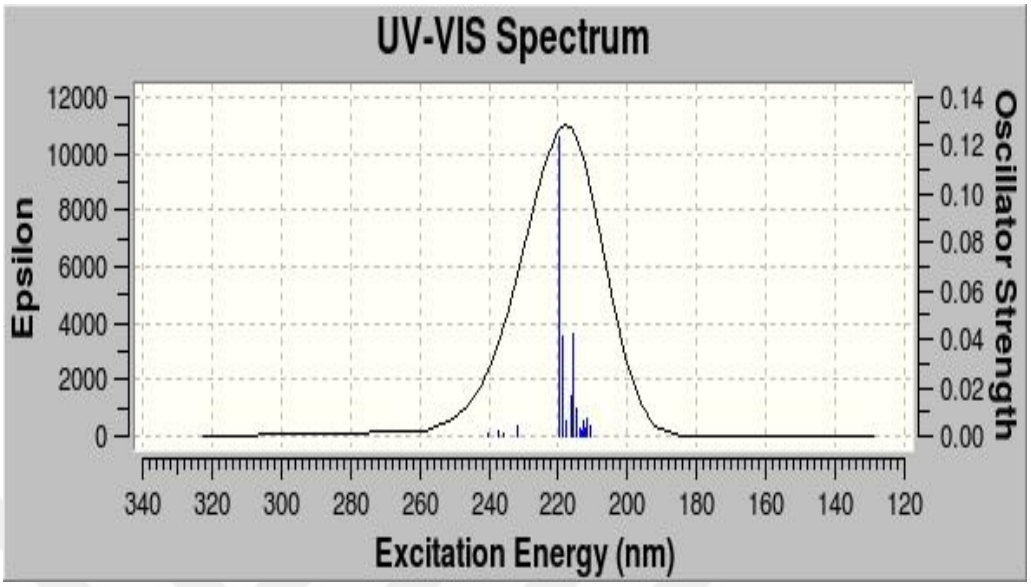

APPENDIX 5. UV-vis spectra of LOPV molecular structure obtained by B3LYP/6-311+G(d, p) method in water environment